A SPECTROSCOPIC INVESTIGATION OF SOME IRON II COMPLEXES

A SPECTROSCOPIC INVESTIGATION OF SOME IRON II COMPLEXES

By

MONICA F. MORRIS, B.Sc.

A Thesis

Submitted to the Faculty of Graduate Studies

in Partial Fulfilment of the Requirements

for the Degree

Master of Science

McMaster University

May 1971

MASTER OF SCIENCE (1971)
(Chemistry)

McMASTER UNIVERSITY
Hamilton, Ontario

TITLE: A Spectroscopic Investigation of Some Iron II Complexes

AUTHOR: Monica F. Morris, B.Sc. (University of British Columbia)

SUPERVISOR: Dr. T. Birchall

NUMBER OF PAGES: x, 111

SCOPE AND CONTENTS:

A number of complexes FeX_2L_n (X = Cl, Br; L = formamide, N-methylformamide, N,N-dimethylformamide, acetamide, benzamide, isobutyramide, urea, N-methylurea, N,N'-dimethylurea, thioacetamide, thiourea, N-methylthiourea, N,N'-dimethylthiourea, benzothiazole, aniline) have been prepared and investigated by means of Mossbauer and infrared spectroscopy and magnetic measurements. It has been possible to distinguish firstly between 4-coordinate and 6-coordinate complexes and secondly between a number of different types of 6-coordinate complexes.

ACKNOWLEDGEMENT

The author is grateful for help and direction from her supervisor, Dr. T. Birchall. Valuable assistance with the Mossbauer fitting and plotting programs was given by Ian Drummond. Beryl Speiers and Bill Courrier are thanked for helping with the far infrared and magnetic measurements. The author's husband, Trevor, is thanked for drawing some of the diagrams. Gratitude is expressed for a graduate student assistantship from the Department of Chemistry at McMaster University.

TABLE OF CONTENTS

LIST OF TABLES

LIST OF FIGURES

CHAPTER I

Introduction and Theory

Purpose of the Investigation

Divalent iron has a d^6 electronic configuration. In a weak crystal field it has one electron outside a half-filled d-shell. In an octahedral field the d-orbitals split to give a lower triplet t_{2g} and an upper doublet e_g, separated by an energy 10Dq of (1) 10,000 to 12,000 cm^{-1} (Fig. 1).

Figure 1.

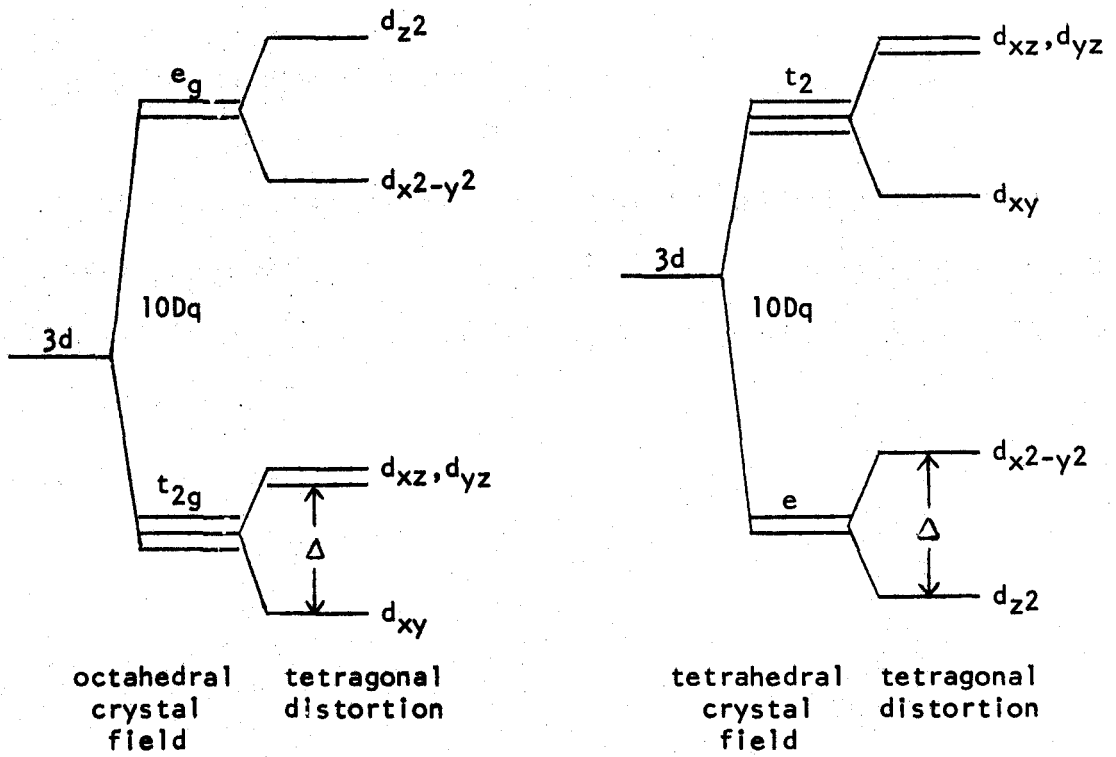

The crystal field stabilization energy of 4Dq is seen to be of the order of 4,000 to 5,000 cm^{-1}. In a tetrahedral crystal field the d-orbitals split into a lower doublet e and an upper triplet t_2, separated by an energy 10Dq of 3,000 to 6,000 cm^{-1}(2). In this case the crystal field stabilization energy of 6Dq is about 2,000 to 4,000 cm^{-1}. Divalent iron, then, can be satisfactorily stabilized by either an octahedral or a tetrahedral environment. The octahedral environment is more energetically favorable, and indeed is much more common for iron II. However, although a tetrahedral environment is less favorable because of a smaller effective crystal field, it should be more favorable from the point of view of smaller metal-ligand distances. This effect should be particularly enhanced by polarizable ligands such as bromide ion, iodide ion, ligands coordinating through sulfur, etc. Chan et al (3) have shown that dichlorobisbenzothiazoleiron II has octahedral coordination about iron whereas the bromo analogue has tetrahedrally coordinated iron. The present study will show that complexes with sulfur coordinating ligands about iron II are almost invariably tetrahedral.

For both octahedral and tetrahedral iron II complexes, some degree of Jahn-Teller distortion would be expected to further split the 3d energy levels and increase the crystal field stabilization energy (Fig. 1). Distortion of this type results in a splitting of the $^5T_{2g} \rightarrow {}^5E_g$ band in the electronic spectra of such complexes as $Fe(H_2O)_6^{2+}$ (4). Jahn-Teller distortion can also be detected by the presence of a large quadrupole splitting in the Mossbauer spectrum. Gibb and Greenwood (5) reported a room temperature quadrupole splitting for the tetrachloroferrate II ion of 1.63 mm/sec. This was the first reported evidence for the distortion expected in a tetrahedral high spin d^6 complex.

Relatively few tetrahedral complexes of iron II are known. The $[FeX_4]^{2-}$ ions, where X = Cl, Br, NCS, etc., have been found to exist with large cations and have been characterized by their electronic spectra (6-8) and more recently by Mossbauer spectroscopy (5, 9). Complexes of the type FeX_2L_2 are also known in which L = pyridine and substituted pyridines (1), triphenylphosphine (10-12), triphenylarsine (2), quinoline and 3-methylisoquinoline (13), benzothiazole (3), thioacetamide (14-16) and thiourea (17). The majority of divalent iron compounds are octahedral. It was of much interest, then, when Singh and Rivest (18) reported the preparation of a series of "tetrahedral" complexes $FeCl_2L_2$ where L = formamide, N-methylformamide and acetamide. However, in the light of a Mossbauer investigation, Birchall (19) suggested that these are polymeric chlorine bridged species with octahedral coordination about iron.

It was the purpose of the present work to follow up this preliminary investigation in order to obtain more structural information and to attempt to prepare complexes of stoichiometry FeX_2L_2 which are indeed tetrahedral. The complexes studied fall roughly into two structural groups, those in which the iron is six-coordinate and those with tetrahedrally coordinated iron. The octahedral group consists of dichloroiron II complexes with the ligands formamide, N-methylformamide, N,N-dimethylformamide, acetamide, isobutyramide, benzamide, urea, N-methylurea, N,N'-dimethylurea, aniline, benzothiazole and thiourea. Dibromoiron II complexes with N,N'-dimethylurea and aniline also fall into this category. Evidence will be presented which shows that the complexes in this group are for the most part chlorine bridged dimers or polymers. A thiourea

complex FeX_2L_2 which is monomeric, an N-methylurea complex which has been formulated as $[FeL_6]Cl_2$, and an isobutyramide complex which contains both six and four coordinate iron II and has been formulated as $[FeL_6][FeCl_4]$ are exceptions. Dichloroiron II complexes with thioacetamide, thiourea, N-methylthiourea and N,N'-dimethylthiourea, and dibromoiron II complexes with thioacetamide, thiourea and benzothiazole will be shown to be four coordinate and monomeric.

The Mossbauer Effect

The Mossbauer effect is the recoilless emission and resonant reabsorption of gamma rays which arise from nuclear excited states. The importance of the effect is that it gives energy quanta which are much more precise than any previously known energy quanta. Mossbauer gamma rays can be used to detect minute changes in the nuclear energy levels, and resolve electron-nuclear hyperfine interactions.

When a nucleus undergoes a transition from state E_e to state E_g by the emission of a photon, the conservation of momentum requires that the momentum of the nucleus, p_M, recoiling in one direction is equal and opposite to the momentum of the photon, p_γ, emitted in the opposite direction. The kinetic energy of the recoiling nucleus is E_R, so that for a nucleus of mass M and velocity v,

$$E_R = 1/2\ Mv^2 = p_M^2/2M \tag{1}$$

The momentum of a photon of zero rest mass is related to the energy by

$$E_\gamma = p_\gamma c \tag{2}$$

Since the two momenta must be equal it follows that

$$E_R = E_\gamma^2/2Mc^2 \tag{3}$$

Thus E_γ will be less than the transition energy, $E_t = E_e - E_g$, by an amount E_R. Similarly, the energy required to populate the E_e state in an absorber will be larger than E_t by the same amount E_R.

The spectral linewidth Γ of a nuclear gamma ray is typically much smaller than the recoil energy E_R of the nucleus. For example, the ^{57}Fe nucleus emits a 14.4 KeV gamma ray with a linewidth $\Gamma = 4.55 \times 10^{-9}$ eV and recoils with energy $E_R = 1.9 \times 10^{-3}$eV. Under normal conditions there will be no overlap of emitted and absorbed lines, and resonance will not occur.

Mossbauer's discovery of recoilless resonant absorption (20, 21) was made when, on cooling an ^{191}Ir source and absorber to 78°K he found a marked increase in the resonant absorption. The opposite effect would have been expected, since a decrease in temperature would decrease the linewidth Γ of the gamma line. Mossbauer realized that the large resonance overlap implied by the increase in resonant absorption was due to an appreciable fraction of the emission and absorption events occuring with no recoil energy loss. This happens because the effective recoiling mass M has become the mass of the whole crystal lattice. This effect is explained by the Debye theory of solids (22), and leads to the premise that recoilless resonance should be observable whenever the Debye temperatures of source and absorber are sufficiently high with respect to the temperatures at which emission and absorption occur. The basic physics of the Mossbauer effect are discussed in detail by Boyle and Hall (23).

In a typical Mossbauer experiment the absorbing nuclei are in a different chemical environment to that of the emitting nuclei, and so the nuclear energy levels are not identical. In order to observe resonant absorption the energy of the emitted gamma ray is systematically varied. In this study a vibrating drive system was used to impart a constantly varying Doppler shift to the emitted gamma rays. The Mossbauer spectrum consists of a plot of gamma ray count vs relative velocity of source to absorber. At some velocity there is resonant absorption and a drop in count rate.

Magnitude of the Effect

The magnitude of the resonance effect depends on the probabilities of recoil free emission and absorption. It also depends on the number of absorber nuclei in the optical path. ^{57}Fe has a rather low isotopic natural abundance of 2.17%, but has a large recoil free fraction, making isotopic enrichment unnecessary except in studies of some very high molecular weight biological materials.

A third factor determining the resonance effect magnitude is temperature. The temperature dependence can be derived in the following way. The recoil free fraction f is related to the mean square amplitude of vibration $\langle x^2 \rangle$ by the equation

$$f = \exp\left(-4\pi^2 \langle x^2 \rangle \frac{E_\gamma^2}{h^2 c^2}\right) \tag{4}$$

in which E_γ is the energy of the gamma quantum involved. The value of $\langle x^2 \rangle$ for the atom involved in the emission or absorption can be derived from the Debye theory of specific heats (24). In this model the Debye temperature Θ_D is defined as

$$\Theta_D = \frac{h\omega_{max}}{k} \tag{5}$$

where ω_{max} is the maximum oscillator frequency of the atom in the lattice, from which

$$f = \exp\left(-\frac{3E_R}{2\Theta_D k}\left\{1 + \frac{2\pi^2}{3}\frac{T^2}{\Theta_D}\right\}\right) \tag{6}$$

when $T << \Theta_D$. As $T \to 0$, the recoil free fraction depends only on the ratio of the recoil energy E_R to the Debye temperature, so that substituting Eq 3 for E_R we have

$$f = \exp\left(-\frac{3E\gamma^2}{4Mc^2k\Theta_D}\right) \tag{7}$$

in the low temperature limit.

As the temperature is increased, the term $T^2/\Theta_D{}^2$ becomes appreciably large and reduces the value of f by the factor e^{-T^2}. For many compounds of iron Θ_D is sufficiently large that resonance absorption is observable at room temperature.

Isomer Shift

The Mossbauer parameter which yields the greatest amount of chemical information is the isomer shift, defined as the displacement from zero relative velocity of the resonance maximum, or of the centroid of the resonance spectrum in the case of spectra with hyperfine structure. The isomer shift arises from the fact that the nucleus of an atom occupies a finite volume. It is surrounded and penetrated by electronic charge with which it interacts electrostatically. The energy of interaction can be computed classically by considering a uniformly charged spherical nucleus imbedded in its s-electron charge cloud. A change in the s-electron density such as would arise from a change in the covalency of metal-ligand bonds, will result in a shift in the nuclear energy levels. A derivation of this shift follows. To simplify the calculation, the difference between the electrostatic interaction of a hypothetical point nucleus and one of actual radius R, both having the same charge, is computed. A point nucleus of atomic number Z gives rise to an electrostatic potential at a distance r of $V = -Ze/r$. For a finite sized nucleus of radius R the potential will be identical to that of a point nucleus for $r > R$, but equal to

$$V' = - Ze/r \mid 3/2 - r^2/2R^2 \mid \qquad (8)$$

for $r < R$. An electron cloud of uniform density ρ interacting with the nuclear charge will give rise to a perturbation energy in the hypothetical case of $E = \int_0^\infty \rho V 4\pi r^2 \, dr$ and in the actual case of $E = \int_0^\infty \rho V' 4\pi r^2 \, dr$. The energy difference is

$$\delta E = \int_0^\infty \rho (V' - V) \, 4\pi r^2 \, dr = 4\pi\rho Ze/R \int_0^R (- 3/2 + r^2/2R^2 + R/r) \, r^2 \, dr$$

$$= 2/5 \, \pi\rho ZeR^2 \qquad (9)$$

Since the electron density at the nucleus is appreciably large only for s-electrons, ρ can be approximated by $|\Psi s(0)|^2 e$, giving

$$\delta E = 2/5\ \pi Z e^2 R^2\ |\Psi s(0)|^2 \tag{10}$$

Nuclear ground states and excited states do not have equal radii for equivalent charge distribution. The gamma ray energy observed is

$$\Delta(\delta E) = 2/5\ \pi Z e^2\ |\Psi s(0)|^2 (R_e^2 - R_g^2) \tag{11}$$

At this point the contribution to δE from the point nucleus drops out. In the approximation used $|\Psi s(0)|^2$ is assumed to remain constant in this step. In practice, $\Delta(\delta E)$ is not measurable by itself, but is usually evaluated with respect to a given absorber-reference pair.

$$\Delta|\Delta(\delta E)| = 2/5\ \pi Z e^2 (R_e^2 - R_g^2)\{|\Psi s(0)|_a^2 - |\Psi s(0)|_{ref}^2 = IS \tag{12}$$

This approximates to

$$IS = \text{constant} \cdot \delta R/R \cdot \Delta|\Psi s(0)|^2 \tag{13}$$

The sign of $\delta R/R$ is negative for ^{57}Fe since the nuclear radius decreases on excitation to the 3/2 spin state. Consequently the isomer shift has a negative dependence on the s-electron density in iron complexes. An immediate application of this relationship is the determination of the oxidation state of iron. The 3d-electrons screen the 4s-electrons from the nuclear charge. In iron II this screening is more effective than in iron III due to the extra 3d-electron. The inner s-orbitals are expanded more, and the nucleus experiences a smaller s-electron density and a larger isomer shift. In the absence of other complicating factors isomer shifts in the range 0.5 to 0.8 mm/sec have been found characteristic of iron III and shifts between 1.0 and 1.7 mm/sec characteristic of iron II.

Second Order Doppler Shift

The nuclear isomer shift is not the only effect which can cause a resonance line shift. Thermal vibrations in the crystal lattice give rise to a second order Doppler effect. A shift to lower energy of the gamma quantum is therefore expected as the temperature increases, with a temperature coefficient per degree (25, 26) of

$$\delta E_\gamma / E_\gamma = Cp/2c^2 \qquad (14)$$

where Cp is the specific heat of the solid. This effect is of little chemical interest, but is observed in studies in which the source temperature is constant while that of the sample is varied. In single temperature comparisons the contribution of the thermal second order Doppler shift to the total resonance energy shift is usually ignored, and observed shifts are interpreted solely as nuclear isomer shifts.

Quadrupole Splitting

If a nucleus is not spherical, or does not have a uniform charge density, effects appear which are higher order terms in the multipole expansion of the electrostatic interaction between nuclear charge and electronic environment. These effects lift the (2I + 1) - fold degeneracy of the nuclear state. A non-spherically symmetric nucleus, i.e. a nucleus with spin greater than 1/2, has a quadrupole moment, Q, which can interact with an electric field gradient at the nucleus. The presence of a non-zero field gradient at the nucleus is determined primarily by the distribution of electrons about the nucleus, which in turn is dependent on the symmetry of the bonding about the atom in question. If the electric field due to the electrons about the nucleus is spherical, as in the case of a filled or half-filled shell configuration, the lattice contribution to the electric field may become important. In such a case a lattice of less than cubic arrangement about the Mossbauer atom will produce a non-zero field gradient at the nucleus. The field gradient can be specified by three components $\delta^2V/\delta x^2 = Vxx$, $\delta^2V/\delta y^2 = Vyy$ and $\delta^2V/\delta z^2 = Vzz$. These are not independent, but must obey the Laplace equation $Vxx + Vyy + Vzz = 0$ in a region where the charge density vanishes. The charge density of the s-electrons does not vanish at the nucleus, but since the s-electrons have a spherically symmetric distribution they do not contribute to the field gradient. The two independent components are chosen as Vzz, defined by eq, and η, the asymmetry parameter, defined by $\eta = (Vxx - Vyy)/Vzz$. These components are usually defined so that $|Vzz| > |Vxx| \geq |Vyy|$, making $0 \leq \eta \leq 1$.

The interaction between the nuclear quadrupole moment and the electric field gradient is given by the Hamiltonian

$$H = \frac{eqQ}{4I(2I - 1)} \{ 3I_z^2 - I(I + 1) + \eta/2(I_+^2 + I_-^2) \} \qquad (15)$$

where I_+ and I_- are shift operators. Equation 15 has eigenvalues

$$E_Q = \frac{eqQ}{4I(2I - 1)} \{ 3m_I^2 - I(I + 1) \} (1 + \eta^2/3)^{1/2} \qquad (16)$$

A full derivation of these equations is given in a paper by Boyle and Hall (23). Expression 16 contains only the second power of the magnetic quantum number m_I, which means that states whose m_I differ only in sign remain degenerate (Fig. 2).

Figure 2.

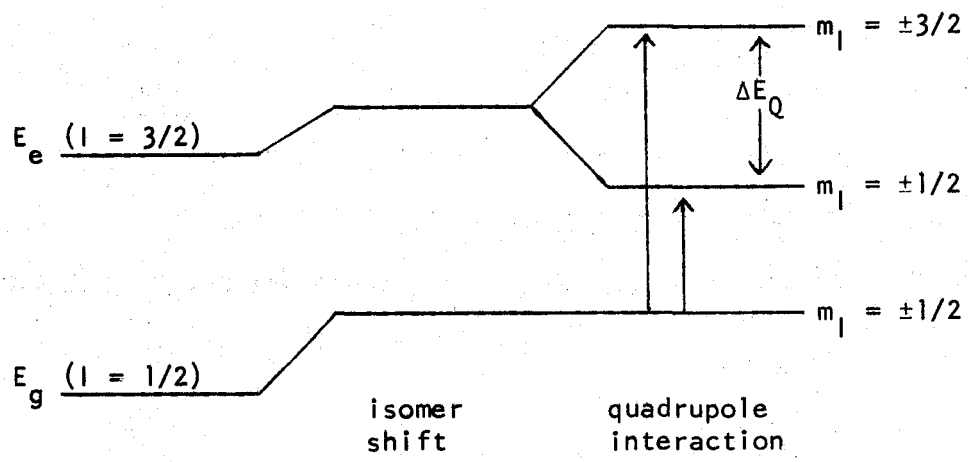

The difference between two eigenvalues calculated from equation 16 for the ground and excited states of the Mossbauer nuclide is the quadrupole splitting.

$$\Delta E_Q = E_Q(m_{Ie}) - E_Q(m_{Ig}) = QS \qquad (17)$$

The origin of the electric field gradient is of interest if quadrupole splittings are to be given chemically significant interpretations.

The two fundamental sources of the electric field gradient are the charges on distant ions and the electrons in incompletely filled shells of the Mossbauer atom. With ^{57}Fe two approaches have been used in interpreting quadrupole splittings. The first is based on measurements of ionic divalent iron salts. In this approach the field gradient is assumed to depend only on the electrons of the atomic shell of the nucleus under consideration. The role of the lattice is simply to provide a crystal field to lift the degeneracy of the d-orbitals of the free ion. In a weak crystal field where Hund's rule is obeyed, divalent iron has one d-electron outside a half-filled shell with spherical symmetry. The entire field gradient, then, arises from this 6th 3d-electron.

The second case is illustrated by ionic trivalent iron ($3d^5$) where smaller quadrupole splittings are found. In a weak crystal field the five 3d-electrons are in a half-filled shell with spherical symmetry which does not contribute to the field gradient. The observed quadrupole splitting must then arise from the field gradient due to other ions in the crystal.

Line Asymmetry

Quadrupole split lines sometimes show unequal intensities. Three factors can cause this effect.

(1) The occurence of a preferential orientation of the absorber crystallites in the sample holder can produce non-random orientations of some crystal axis with respect to the source-detector axis. This effect has been observed in $Fe_2(CO)_9$ by Gibb et al (27). Rotation of a sample of partially oriented $Fe_2(CO)_9$ crystallites resulted in a varying intensity ratio for the two quadrupole split lines. The origin of the non-equivalence of the intensity for resonance lines lies in the angular dependence of this intensity. The angular dependencies for the two lines in a quadrupole split ^{57}Fe spectrum are given below (24),

Transition	$I(\theta)$	$I(\theta)$ for $\theta = 90°$	$I(\theta)$ for $\theta = 0°$
$\pm 3/2 \rightarrow \pm 1/2$	$3/2(1 + \cos^2\theta)$	5	2
$\pm 1/2 \rightarrow \pm 1/2, \mp 1/2$	$1 + 3/2\sin^2\theta$	3	6

where θ is the angle between the axis of symmetry and the optical axis of the experiment. Two results are of interest in these relationships: (i) the maximum difference in $I(\theta)$ for the two lines occurs when the symmetry axis is parallel to the optical axis; and (ii) $\int_0^{2\pi} I(\theta)d\theta$ is equal for the two quadrupole split lines. A consequence of (ii) is that for a finely powdered material packed into an absorber in random orientations, the two lines should be of equal intensity.

(2) A second source of line asymmetry comes from the angular anisotropy of the probability of emission or absorption of a quantum in a recoil free

transition. This is commonly referred to as the Goldanskii Effect (28, 29) but was originally given mathematical formulation by Karyagin (30). The probability of a recoil free transition is related to the mean square amplitude of vibration $\langle x \rangle^2$ by the equation

$$f = \exp\ (-4\pi^2 \langle x \rangle^2 / \lambda^2) \qquad (18)$$

where λ is the wavelength of the radiation and the value of $\langle x \rangle^2$ is averaged over the transition lifetime. Since $\langle x \rangle^2$ is dependent on the strength of the chemical bond in a given direction, there will be an angular dependence of the recoil free fractions for emission and absorption, and hence of the two $I(\theta)$ functions. In cases where there is a large asymmetry in the chemical bonding, as when ligands in one direction are strongly π-bonding while those in the other direction are σ-bonded, or where large differences in electron donating or withdrawing power exist, the asymmetry is expected to be especially pronounced. This asymmetry persists even when there is random orientation of the crystal axis with respect to the optical axis. The effect should increase with temperature.

(3) Asymmetric quadrupole split lines can also arise as a result of the fluctuating electric and magnetic fields produced by relaxation of paramagnetic ions, or by fluctuation of the environment around the nucleus (31). Consider ^{57}Fe in a fixed electric field gradient along the z-axis which arises from distant charges. It has nuclear energy levels such as those shown in Fig. 2. For an isotropic polycrystalline sample in the absence of an anisotropic probability of absorption, the two lines should have equal intensity. But assume that the ion is in an electronic state with, for example, S = 1/2. As the ion makes electronic transitions

between the +1/2 and -1/2 states, the internal field jumps between the values $+h_o$ and $-h_o$ along the z-axis, where for iron h_o can be of the order of several hundred kilogauss. If the fluctuation rate is slow compared to the precession frequency of the nucleus in h_o, a full six-line hyperfine spectrum such as that in Fig. 4 should be observed. If the fluctuation rate is rapid the nucleus will see only the time averaged field, which is zero if the ionic states are degenerate, and a symmetric quadrupole pattern will then be observed. However, in the Mossbauer effect there are a number of Zeeman precession frequencies corresponding to the different transitions between magnetic sublevels of the excited and ground nuclear states. The $\pm 3/2 \rightarrow \pm 1/2$ transitions, which make up one of the lines of the quadrupole doublet, have a larger splitting in a magnetic field than do the $\pm 1/2 \rightarrow \pm 1/2$ and $\pm 1/2 \rightarrow \mp 1/2$ transitions which make up the other line. This means that the fluctuations of the paramagnetic ion have a different effect on the two components of the quadrupole split line. In particular, one would expect to find a range of relaxation times in which the $\pm 1/2 \rightarrow \pm 1/2, \mp 1/2$ line is fully narrowed while the $\pm 3/2 \rightarrow \pm 1/2$ line is still broad.

If the fluctuations in internal magnetic field are due to electronic spin-lattice relaxation, we would expect the relaxation times and also the asymmetry to decrease with increased temperature (opposite to the Goldanskii Effect). But if fluctuations are due to electronic spin-spin relaxation, asymmetry will depend on concentration of paramagnetic ions and will be essentially independent of temperature.

Magnetic Hyperfine Structure

In an asymmetric electric field states with magnetic quantum numbers $+m_I$ and $-m_I$ occur at the same energy. This degeneracy can be removed by placing the Mossbauer atom in a magnetic field which arises either internally, as in a ferromagnetic material such as Fe_2O_3, or which is generated by an external magnetic field. Under such conditions a nuclear Zeeman effect is observed in which each nuclear energy level is split into its 2I + 1 components as in Fig. 3.

Figure 3.

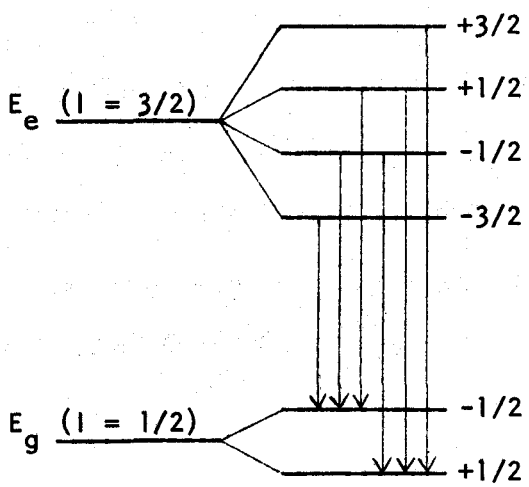

The selection rules for dipole transitions which govern allowed transitions between these levels are $\Delta m_I = 0, \pm 1$, so that in an absorber with an excited state of I = 3/2 and a ground state of I = 1/2, a six line hyperfine structure spectrum will be observed.

Magnetic hyperfine splittings are usually of the same order of magnitude as quadrupole splittings. In the presence of both a magnetic

field gradient and an electric field gradient a ^{57}Fe nucleus could exhibit a six line spectrum such as that shown in Fig. 4. The ±1/2 levels are moved in one direction and the ±3/2 levels in the other. This effect enables the sign of the electric field gradient to be determined. The spacing between the highest velocity pair of lines is greater than that between the lowest velocity pair if the sign of the electric field gradient raises the ±3/2 levels.

Figure 4.

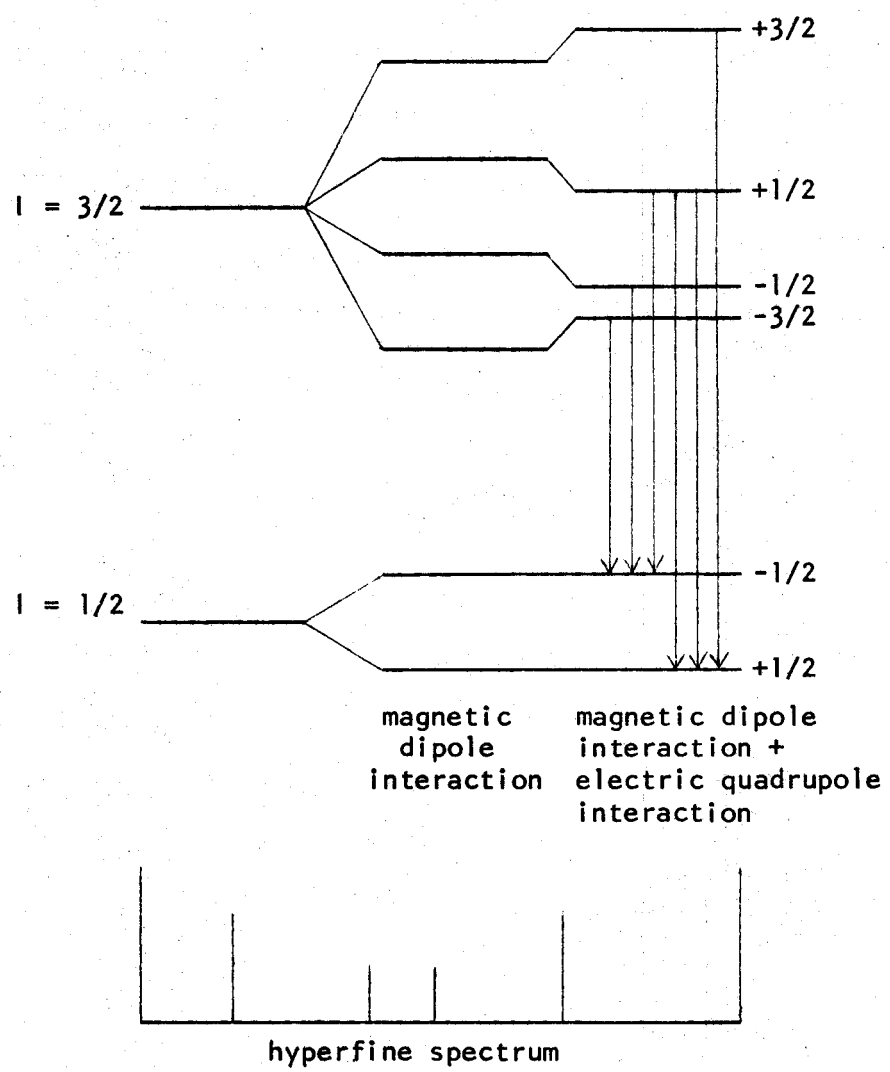

Mossbauer Spectra of Iron II Complexes

The isomer shift and the quadrupole splitting are the Mossbauer parameters of most interest in chemical applications. The isomer shift gives intimate information on the nature of the metal-ligand bonds, and the quadrupole splitting and its temperature dependence relate to the symmetry of these bonds.

(I) Isomer Shift

Expression 13 for the isomer shift involves three terms: a constant term, a nuclear radius term and an electron density term. The radial term has a negative sign (24) and is assumed to be constant in the iron II complexes investigated. Changes in the isomer shift can be considered to arise primarily from changes in the electron density $|\Psi s(0)|_a^2$ at the absorbing ^{57}Fe nucleus. This term is the sum of s-electron densities and will be affected by the extent to which s-orbitals are used in bonding. Two effects will be of interest: (i) the effect of a change in coordination number about iron, and (ii) the effect of a change in s-electron donating properties of the ligands.

Using simple reasoning we can say that in an octahedral environment hybrid orbitals like sp^3d^2 will be of some importance (unless bonding is totally ionic), and in a tetrahedral environment sp^3 hybrid orbitals will be significant. A change from sp^3d^2 to sp^3 hybridization increases the s-character of the bonds by about 10%. The effect is made more pronounced by d-orbital shielding. In the octahedral case, donation of electron density to the 4s-orbital is counteracted by donation of electron density to the 3d-orbitals which effectively screen a portion of the 4s-orbital

from the nuclear charge. This allows expansion of the 4s-electron shell and results in a reduced s-electron density at the nucleus. The contribution due to p-electrons should be very small (24). In the tetrahedral case the increase in s-electron density due to donation by the ligands is not offset by an increase in d-electron density. Thus the iron II nucleus in a tetrahedral environment should experience a significantly greater s-electron density than one in an octahedral environment. This means that $|\psi_s(0)|^2$ is larger in tetrahedral complexes than in octahedral complexes, and we would expect from expression 13, recalling that the sign of $\delta R/R$ is negative, that tetrahedral complexes will show smaller isomer shifts than octahedral complexes. This relationship should be strictly true between complexes differing only in the number but not in the character of the ligands. However, the effect is sufficiently large that it may be applied to many simple iron II complexes. A decrease in isomer shift on lowering the coordination number has been observed by several workers for iron III (32, 33). The effect is also evident in comparing isomer shifts of the tetrachloroferrates (5, 9) and other tetrahedral iron II complexes (13, 34) with isomer shifts of octahedral complexes (19, 35-38). These results show that isomer shifts in the region 0.8 to 1.2 mm/sec are usually characteristic of tetrahedral iron II complexes and shifts in the region 1.2 to 1.7 mm/sec are characteristic of octahedral iron II complexes.

The effect on the isomer shift of a change in the electron donating properties of ligands is evident. A more electronegative ligand will donate less electron density to the iron nucleus than a less electronegative ligand. The isomer shift would therefore be expected to be

greater for a complex with more electronegative ligands than one of the same geometry with less electronegative ligands.

This effect is often enhanced by π-backbonding. Removal of electron density from the 3d-orbitals results in deshielding of the nucleus from 4s-electron density, causing a higher charge density at the nucleus. Smaller isomer shifts would be expected with strongly backbonding ligands. (This π-effect makes the identification of oxidation state more difficult.) An example is sodium nitroprusside, for which an isomer shift of zero is assigned.

(2) Quadrupole Splitting

A ^{57}Fe nucleus has a ground state spin of I = 1/2. Since in this state the nucleus has a zero quadrupole moment there will be no interaction with an electric field gradient. However, the 3/2 excited state will be split into two components as shown in Fig. 2. The difference between the two eigenvalues calculated from equation 17 is the quadrupole splitting.

$$\Delta E_Q = E_Q(\pm 3/2) - E_Q(\pm 1/2) = 1/2eqQ(1 - \eta^2/3)^{1/2} = QS \qquad (19)$$

If the ^{57}Fe nucleus occupies a lattice site which experiences an axially symmetric field such that Vxx = Vyy and η = 0 the quadrupole splitting becomes

$$\Delta E_Q = 1/2eqQ = QS \qquad (20)$$

Let us consider under what conditions quadrupole interaction will be observed in iron II complexes. The electronic configuration of divalent iron is d^6. In a weak octahedral or tetrahedral crystal field

there will be one d-electron outside a half-filled shell with spherical symmetry. The entire field gradient then arises from this sixth 3d-electron. However, if the t_{2g} set in the octahedral case, or the e set in the tetrahedral case are degenerate, the sixth electron will populate equally the orbitals of the set. An equally populated t_{2g} or e set has cubic symmetry, and there will be no contribution to the field gradient. Complexes in which iron II has undistorted octahedral or tetrahedral symmetry are expected to show little or no quadrupole splitting.

If the degeneracy of the d-orbitals is lifted by a distortion as indicated in Fig. 1, the sixth d-electron will preferentially populate the lowest lying orbital(s). This destroys the cubic symmetry present in the undistorted cases and produces a non-zero field gradient. The values of the electric field gradient produced by the different 3d-wavefunctions at the nucleus are given below (39).

Orbital	q	η
$d_{x^2-y^2}$	$+4/7\langle r^{-3}\rangle$	0
d_{z^2}	$-4/7\langle r^{-3}\rangle$	0
d_{xy}	$+4/7\langle r^{-3}\rangle$	0
d_{xz}	$-2/7\langle r^{-3}\rangle$	+3
d_{yz}	$-2/7\langle r^{-3}\rangle$	-3

The magnitude of the quadrupole splitting is taken to be an indication of the degree of distortion from cubic symmetry of the electronic distribution and also of the crystal field due to the ligands.

A secondary contributing factor is covalency in metal-ligand bonds. Since the components Vxx, Vyy and Vzz contain terms in $\langle r^{-3} \rangle_d$ and $\langle r^{-3} \rangle_p$, a change in the radii of the p and d shells will cause a change in the electric field gradient at the nucleus. The expansion of the 3d-orbitals onto the ligands decreases the value of $\langle r^{-3} \rangle_{3d}$. Also, some 4p character may be mixed into the metal-ligand bonds, causing a decrease in the value of $\langle r^{-3} \rangle_{4p}$. Both these mechanisms cause a decrease in the quadrupole splitting (9).

(3) Temperature Dependence of Quadrupole Splitting

In most high spin iron II compounds the ligand field is close to cubic. Thermal electron excitation in the resultant close-lying energy levels produces a temperature dependent electric field gradient at the nucleus. This is manifested in the temperature dependence of the quadrupole splitting in Mossbauer spectra, and gives a means of detecting and measuring small distortions from cubic symmetry.

The value of the quadrupole splitting for any iron compound is given by equation 19. The maximum value of the electric field gradient q which can be produces by a single d-electron is $(1 - R)4/7\langle r^{-3} \rangle_{3d}$ where $(1 - R)$ is the Sternheimer shielding factor and $\langle r^{-3} \rangle_{3d}$ is the mean value of r^{-3} over the radial part of the 3d-wavefunction. Ingalls (39) has expressed observed quadrupole splittings in terms of a QS_{max} and a reduction factor characteristic of the compound and the temperature, as follows:

$$QS = 1/2e^2Q(1 - R)4/7\langle r^{-3} \rangle_{3d}\alpha^2F(\Delta_1,\Delta_2,\lambda,T) \qquad (21)$$

α^2 is a covalency factor introduced to allow for the decrease in $\langle r^{-3} \rangle_{3d}$ on complex formation. It is related to the spin-orbit coupling constant λ by $\lambda = \alpha^2 \lambda_o$ where λ_o is the coupling constant for the free ion, 103 cm^{-1}. Δ_1 and Δ_2 are the distortional splittings in the lower d-orbital set as shown in Fig. 5.

Figure 5.

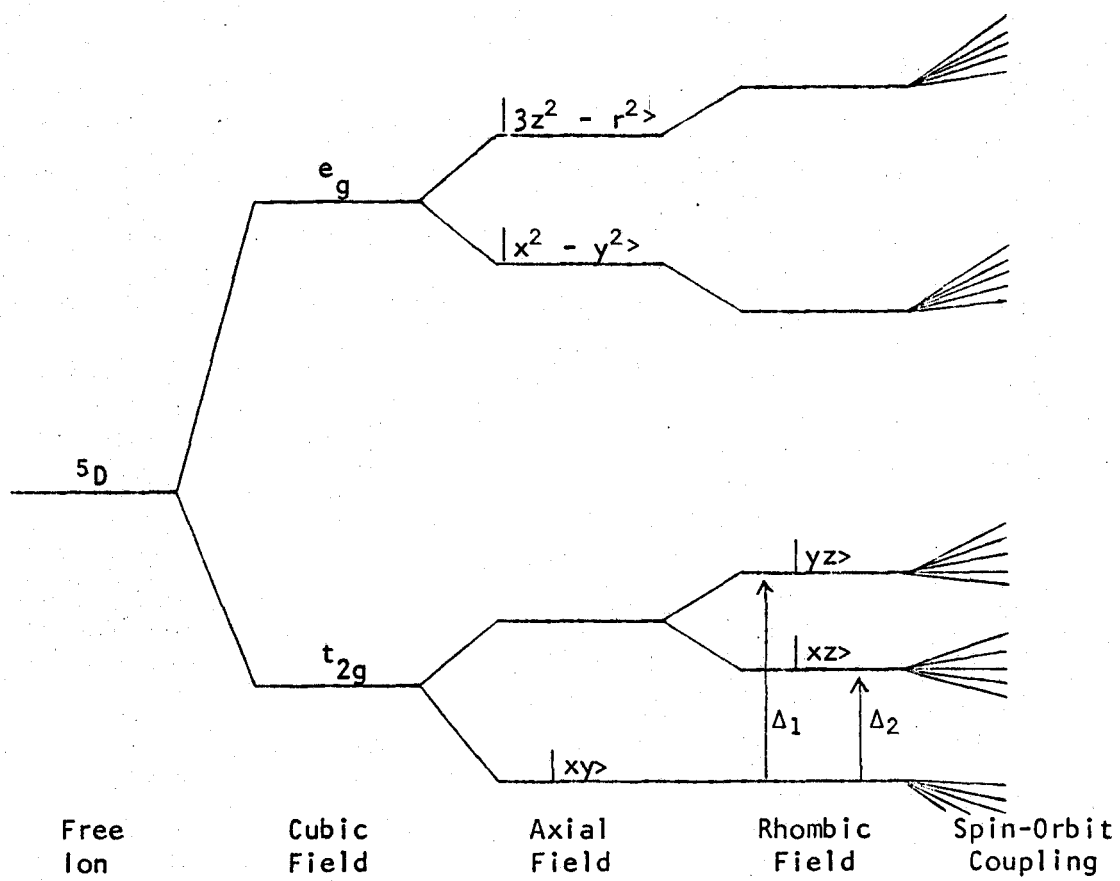

The reduction factor F reflects the effect of the environment on the energies of the 3d shell. This effect can be treated as a perturbation Hamiltonian (40)

$$H = V_o + V_T + V_R + \lambda L \cdot S \qquad (22)$$

V_o is the cubic field term, V_T is the tetragonal (or trigonal) term, V_R is the rhombic term, and $\lambda L \cdot S$ is the spin-orbit coupling. If there are n wave functions which are considered to be important, the n x n matrix can be evaluated as $a_{ij} = \langle \Psi_i | H | \Psi_j \rangle$ and the n eigenvalues and corresponding eigenvectors obtained. The electric field gradients of each energy level can be calculated using the eigenvectors, and the quadrupole splittings obtained by applying a Boltzman Statistical distribution. High spin Fe^{2+} has quantum numbers L = 2 and S = 2, so the five 3d-wavefunctions have 5-fold spin degeneracy. As the spin-orbit coupling constant is of the same order as the d-level splittings and affects the lower levels to the first order this must be considered, so there are $(2L + 1)(2S + 1) = 25$ energy levels. Ingalls (39) has diagonalized the 25 x 25 matrices for a number of ligand field environments and plotted curves relating the reduction factor F to Δ_1, Δ_2, λ and T for the different cases. Gibb (41) has pursued this approach and developed an iterative method for fitting trial models to a set of experimental data obtained from a temperature study of quadrupole splittings.

Since in the present study complete temperature runs were not obtained in the Mossbauer spectra, a thorough treatment such as that described above was not warranted. A simplified model in which rhombic distortion and spin-orbit coupling are ignored will be useful for some of the complexes studied. Gibb and Greenwood (5) used such a model in studying the tetrachloroferrate II ion. Using an approach based on that of Ingalls (39) they calculated the quadrupole splittings of tetrahedral iron compounds to be

$$QS = QS_{max} \frac{[1 - \exp(-\Delta/kt)]}{[1 + \exp(-\Delta/kt)]} \qquad (23)$$

The reduction factor is a function only of the temperature and Δ, the splitting in the e_g levels. Gibb (41) has shown that spin-orbit coupling in tetrahedral iron II compounds is only noticeable at very small distortions and low temperatures, so omission of this parameter in the reduction factor is probably justified. In the present study, errors incurred in the measurement of the quadrupole splittings will be proportionately much greater than that incurred by omitting spin-orbit coupling. The omission of a rhombic term in the reduction factor is also thought to be justified in view of the proposed C_{2v} symmetry of the 4-coordinate complexes. The most interesting feature of this approach is that, as well as Δ values, QS_{max} will be readily obtainable from the quadrupole splitting data, and this term will be chiefly sensitive to the degree of covalency as expressed by α^2.

Burbridge et al (35) have treated some octahedral iron II complexes in an analogous manner, omitting spin-orbit coupling effects and rhombic distortion. Following Ingalls(39) they have expressed the reduction factors as follows. If the orbital singlet lies lowest:

$$F(\Delta,T) = \frac{[1 - \exp(-\Delta/kt)]}{[1 + 2\exp(-\Delta/kt)]} \qquad (24)$$

If the orbital doublet lies lowest:

$$F(\Delta,T) = \frac{[1 - \exp(-\Delta/kt)]}{[2 + \exp(-\Delta/kt)]} \qquad (25)$$

Expected quadrupole splittings are $QS = QS_{max}F(\Delta,T)$. These have been plotted for two temperatures in Fig. 6 to give an idea of the temperature variations in quadrupole splittings which might be expected for different degrees of axial distortion. In calculating these curves QS_{max} has

Figure 6. Plot of QS against Δ_{t2g}.

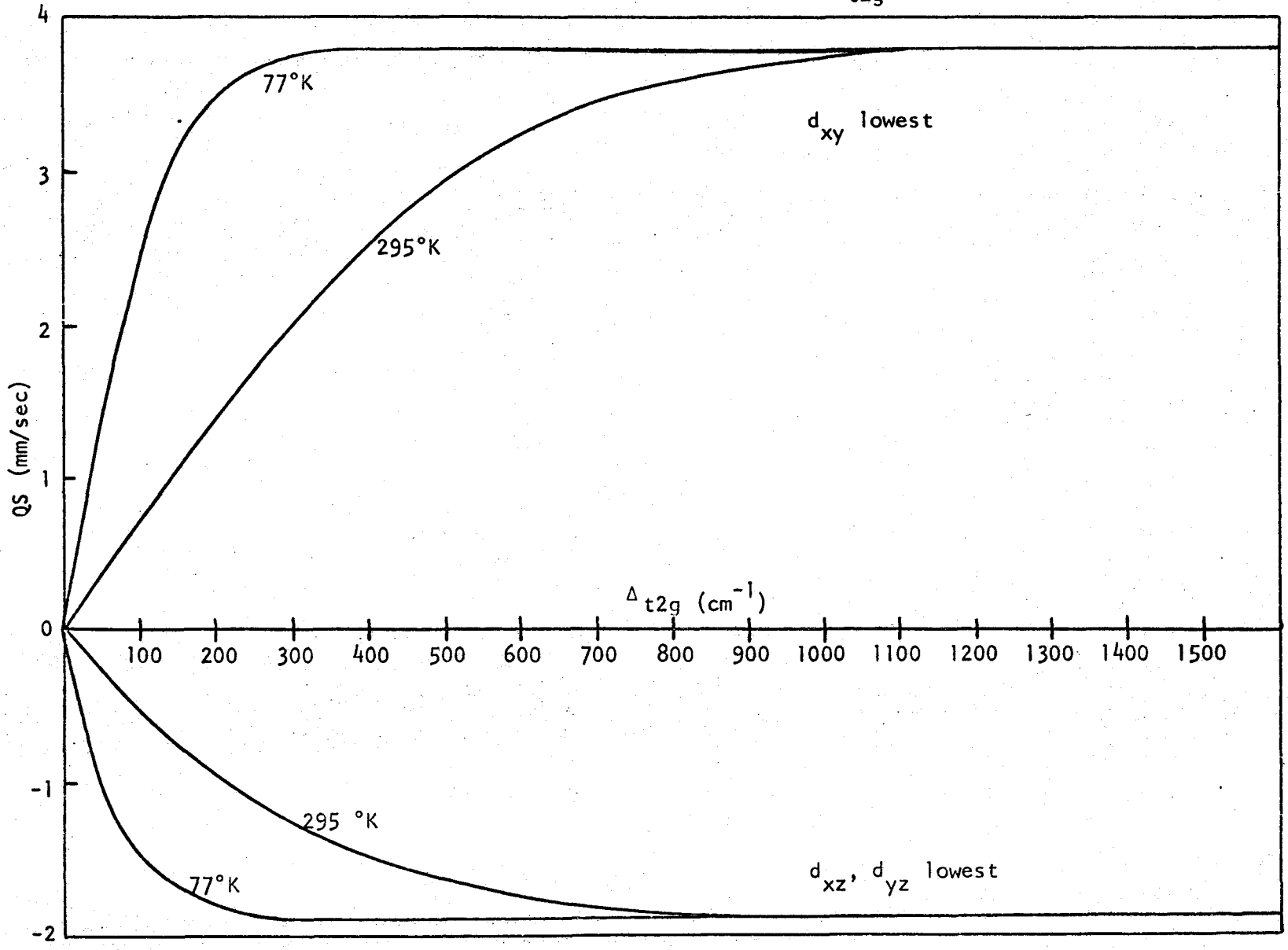

arbitrarily been taken as 3.79 mm/sec, the quadrupole splitting of $FeSiF_6\ 6H_2O$ at 4.2°K (42). This is the highest known value for a ferrous compound.

Burbridge et al (35) have used a curve similar to the one for 295°K in Fig. 6 to estimate tetragonal distortions. But, as Gibb (41) has pointed out, spin-orbit effects in octahedral complexes are significant, and can lead to as much as a 10% reduction in F even at room temperature and distortions as large as 1000 cm^{-1}. At lower temperatures and smaller distortions the errors are much larger. The results in this study have shown that indeed almost none of the observed temperature shifts in quadrupole splittings fit the curves of Fig. 6. Some qualitative conclusions will be drawn nevertheless.

Infrared Spectra, 200 to 400 cm^{-1}

The metal-halogen, metal-oxygen, metal-sulfur, etc., stretching vibrations in transition metal complexes fall mainly in the 200-400 cm^{-1} region of the infrared. Some investigators (43, 44) have drawn correlations between number and frequency of vibrations in this region and the stereochemistry of the complex. Far infrared spectroscopy is a particularly useful technique in studying complexes such as those of iron II. Electronic spectra of these complexes in solution would be difficult to obtain because of their tendency to change form; the polymeric species especially tend to break up in solution. Reflectance spectra of solid samples have been obtained by some investigators (10, 13, 14).

Table I shows the infrared active stretching vibrations expected for some stereochemical types which will be important in this study. It is understood that these vibrations will in general be coupled with bending and deformation modes.

Table I. Distribution of Normal Modes of Vibration in Compounds of Stoichiometry MX_mL_n*

Type	Stereochemistry	Symmetry Group	ν(M-X)	IR Active	ν(M-L)	IR Active
MX_4	Tetrahedral	Td	a_1+t_2	1	—	—
MX_2L_2	Tetrahedral	C_{2v}	a_1+b_1	2	a_1+b_2	2
MX_6	Octahedral	O_h	$a_{1g}+e_g+t_{1u}$	1	—	—
MX_2L_4	trans-Octahedral	D_{4h}	$a_{1g}+a_{2u}$	1	$a_{1g}+b_{1g}+e_u$	1
MX_2L_4	cis-Octahedral	C_{2v}	a_1+b_1	2	$2a_1+b_1+b_2$	4
MX_2L_2	Polymeric Octahedral	C_i	$2a_g+2a_u$	2	a_g+a_u	1

*Calculated by the methods described by E. B. Wilson, J. C. Decius and P. C. Cross, "Molecular Vibrations", McGraw-Hill Book Co., New York, N.Y.

(1) Tetrahedral Complexes

Tetrahedral anions MX_4^{n-} have been studied by Clark and Dunn (45) and Sabatini and Sacconi (46). When the ion is undistorted from tetrahedral symmetry, only one M-X stretching vibration is observed. Some representative frequencies for tetrahedral iron species are given in Table II. The ν(M-X) vibrations clearly depend on X. For the first row transition metals, $\nu(M-Br)/\nu(M-Cl) \simeq 0.77$ is thought to be a rough guide to the magnitude of this dependence in tetrahedral anions MX_4^{n-} (45, 46). Splitting of the triply degenerate t_2 vibration can result from deviation from perfect tetrahedral symmetry or from next nearest neighbor interactions.

For molecules of the type MX_2L_2, two ν(M-X) vibrations and two ν(M-L) vibrations are expected to be infrared active (Table I). The far infrared spectra of MCl_2py_2, where M = Co, Zn and py = pyridine, are given in Table II. They are characterized by two strong bands and one medium band in the 200-400cm^{-1} region (44). The former two bands are assigned as ν(M-X) because they shift down to about 0.77 of their values in the analogous bromo derivatives. The frequency of the third band is almost independent of halogen and is accordingly assigned as a ν(M-L) vibration. The second ν(M-L) vibration is thought to be either too weak to locate or to lie below 200 cm^{-1} (44). Far infrared studies have also been made of some tetrahedral thioacetamide (14) and thiourea (47) complexes, and some of these results have been included in Table II for comparison.

(2) Octahedral Complexes

A regular octahedral species MX_6 or ML_6 has a centre of symmetry, and a mutual exclusion rule applies between normal vibrational modes allowed in the infrared and in the Raman spectra. Only the ν_3 stretching mode of t_{1u} symmetry is expected to be infrared active.

Table II. Infrared Absorption Frequencies, 200-400 cm^{-1}, of Some Tetrahedral Transition Metal Complexes

Compound	ν(M-X)	ν(M-L)	Reference
$[Et_4N^+]_2[FeCl_4^{2-}]$	282 s	—	35
$[Et_4N^+]_2[FeBr_4^{2-}]$	216 s	—	35
$[Ph_3MeAs^+]_2[FeCl_4^{2-}]$	272 s, 286 m, 298 sh	—	35
$[Et_4N^+][FeCl_4^-]$	378 s	—	35
$[Et_4N^+][FeBr_4^-]$	290 s	—	35
$ZnCl_2py_2$	329 s, 296 s	220 m	34
$ZnBr_2py_2$	254 s, (220 m)	(220 m)	34
$CoCl_2py_2$	344 s, 304 s	252 m	34
$CoBr_2py_2$	274 s, 242 m	250 sh	34
$ZnCl_2(THA)_2$	298 s, 275 s	237 sh, 224 ms	11
$ZnBr_2(THA)_2$	(243 m, 224 sh, 212 s, 193 m)*		11
$CoCl_2(THA)_2$	320 s, 294 s	242 ms	11
$CoBr_2(THA)_2$	(266 m, 247 s, 239 s, 193 w)		11
$FeCl_2(THA)_2$	324 s, 302 s	230 ms	11
$FeBr_2(THA)_2$	(259 s, 248 s, 231 s, 226 sh)		11
$ZnCl_2(THU)_2$	(266 s, 255 s, 235 s)		53
$ZnBr_2(THU)_2$	200 s, 185 s	259 s, 240 s	53
$CoCl_2(THU)_2$	314 s, 292 s	278 sh, 249 s	53
$CoBr_2(THU)_2$	235 s, 227 sh	274 s, 251 s	53

py = pyridine, THA = thioacetamide, THU = thiourea
s = strong, m = medium, w = weak, sh = shoulder

*Bands given in brackets are probably strongly coupled ν(M-X) and ν(M-L)

An octahedral complex of the type MX_2L_4 could in general be cis or trans with respect to the positions of the two halogens. As seen from Table I these two species could possibly be identified from the number of infrared stretching bands. Clark and Williams (44) cite some pyridine complexes MX_2py_4 as examples. Trans complexes such as $NiCl_2py_4$, $CoCl_2py_4$ and $IrCl_2py_4^+$ show two distinct bands in the 200-400 cm^{-1} region assigned as ν(M-X) and ν(M-L). In contrast, cis-$IrCl_2py_4^+$ shows a more complicated spectrum with two ν(M-L) bands, a splitting of the ν(M-X) band and a further unassigned band.

Iron complexes $FeCl_2py_4$ and $FeCl_2py_4 \cdot 2py$ show a band at 282 cm^{-1} assigned as ν(Fe-Cl) and a weak band at about 390 cm^{-1} assigned as ν(Fe-N) (48). These complexes are probably trans-octahedral.

A polymeric halogen bridged octahedral complex of stoichiometry MX_2L_2 is expected to show two ν(M-X) stretches and one ν(M-L) stretch in the infrared (Table I). Clark and Williams (44) state that a series of such complexes MCl_2py_2 (M = Mn, Fe, Co, Ni) gives far infrared spectra with badly resolved bands in the 200-260 cm^{-1} region. The appearance of ν(M-Cl) bands in this region makes these spectra strikingly different from the tetrahedral MCl_2py_2 spectra which show well resolved ν(M-Cl) bands in the 300 cm^{-1} region. This shift is expected as a result of longer, weaker bridging halogen bonds in the polymer.

Infrared Spectra, 400-4000 cm^{-1}

Organic ligands absorb in the 400-4000 cm^{-1} region of the infrared. By observing the magnitudes and directions of shifts in peaks due to co-ordination with a metal, the coordinating atom can be inferred.

(1) Amide and Urea Complexes

Amides and ureas both show strong "Amide I" bands due to carbonyl absorption. Unsubstituted amides and ureas generally absorb near 1690 cm^{-1} whereas N-substituted species absorb at slightly lower frequencies. The N-H stretching frequencies of amides and ureas fall in the 3400-3500 cm^{-1} region. Tertiary amides, of course, do not absorb in this region. The N-H stretching bands can show shifts of 100 to 200 cm^{-1} to lower frequencies as a result of hydrogen bonding. Lee and Kumler (49) observe such shifts for acetamide and formamide when they record infrared spectra as KBr discs and in dilute CCl_4 solution. They also observe smaller shifts in the carbonyl stretching frequencies, and suggest that the hydrogen bonding occurs as shown below.

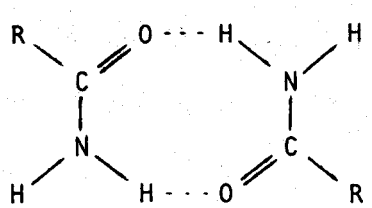

Amides and ureas show a characteristic band, the "Amide II" band, at 1550-1650 cm^{-1}, which is usually attributed to NH_2 bending. Penland et al (50) suggest that in urea the "Amide I and II" bands are not separable, but that the absorptions at 1683 and 1603 cm^{-1} should be considered as coupled vibrations involving both C=O stretching and NH_2 bending. Two

bands, usually attributable to C-N stretching mixed with some NH_2 bending character, are also observed. Stewart (51) assigns these bands at 1468 and 1005 cm^{-1} for urea; Jones (52) assigns them at 1494 and 1200 cm^{-1} for N-methylformamide, while Evans (53) assigns only one band at 1299 cm^{-1} as ν(C-N) for formamide.

Amides and ureas could conceivably coordinate through either oxygen or nitrogen. However, amides usually coordinate through oxygen. This type of coordination should increase the resonance stabilization in the ligand due to polar structures such as the following.

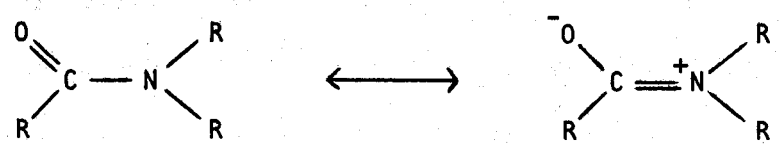

Singh and Rivest (18) have found that in the complexes $FeCl_2L_2$ (L = formamide, N-methylformamide, and acetamide) the amides in each case coordinate through oxygen. These workers noted a negative shift of the carbonyl stretching frequency and a positive shift of the C-N stretching frequency on complex formation. A negative shift in the NH_2 bending or "Amide II" band on coordination also indirectly supported their conclusion, as coordination through nitrogen would cause a positive shift in this band (54). They also noted a marked negative shift in the N-H stretching frequency, which would have been expected for coordination through nitrogen but not through oxygen. This shift has been interpreted as due to hydrogen bonding between the NH_2 hydrogens of the amide and the chlorine of the metal halide. Such hydrogen bonding has been observed by Chatt et al (55) in a series of amine complexes of platinum II chloride.

Urea has been found to coordinate through both oxygen and nitrogen (50). Coordination through oxygen is anticipated from the nature of the polar resonance structures for urea. Vaughan and Donohue (56) considered the structure of urea to involve resonance between the three following structures, the observed values of the interatomic distance indicating 30% double bond character for the carbon-to-nitrogen bonds leaving 40% for the carbon-to-oxygen bond.

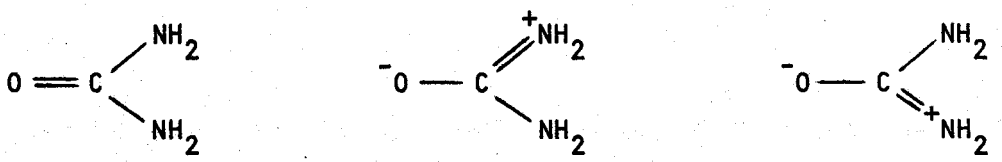

Penland et al (50) find that in the complexes $[Fe(UREA)_6]Cl_3$, $[Cr(UREA)_6]Cl_3$, $ZnCl_2(UREA)_2$ and $CuCl_2(UREA)_2$ coordination occurs through oxygen. Contrary to the observation of Singh and Rivest (18) they observe little change in the N-H stretching region upon complex formation. However, they appear to have recorded the ligand spectrum as a mull and not taken into account the negative shift already present in this region due to hydrogen bonding. Peaks in the C=O stretching and NH_2 bending region are shifted to lower frequency and peaks of C-N stretching character are shifted to higher frequency.

Coordination of urea can also occur through nitrogen, by delocalization of the unshared pair of nitrogen valence electrons to form a weak π-bond. Penland et al (50) observe coordination through nitrogen in the complexes $PdCl_2(UREA)_2$ and $PtCl_2(UREA)_2$. In the N-H stretching region two bands are observed similar to those found in the spectrum of urea, and two additional bands are found at lower frequencies and are assigned to the N-H stretching vibrations of the coordinated NH_2 group. A carbonyl

stretching band is found at 1725 cm^{-1}, indicating a positive shift of about 40 cm^{-1} from the nearest ligand band. This shift is expected to occur upon coordination through nitrogen for two reasons: the formation of N→M bonds increases the electron demand by the donor nitrogen and blocks the resonance between this nitrogen and the carbonyl group. Both these factors bring about increased C=O double bond character. A band at 1590 cm^{-1} is attributed to NH_2 bending of the coordinated NH_2 group, and a shoulder at 1615 cm^{-1} is assigned to bending of the free NH_2 group.

Rivest (57) has studied complexes of titanium tetrachloride with urea, 1,1-diphenylurea and 1,3-diphenylurea. Coordination occurs through oxygen in all cases, resulting in a negative shift of the carbonyl and NH_2 bending vibrations. Aggarwal and Singh (58-60) prepared some stannic halide complexes with amides and ureas. Their infrared spectra show negative carbonyl shifts in all cases, indicating coordination through oxygen.

(2) Thioamide and Thiourea Complexes

Thioamides and thioureas have infrared spectra which are similar to those of amides and ureas in the ν(N-H) and $\delta(NH_2)$ regions. However, there is no strong band due to C=S stretching which is analogous to the carbonyl absorption in amides and ureas. For thioacetamide Suzuki (61) assigns a band at 975 cm^{-1} to a mixture of ν(C-C), $\rho(CH_3)$ and ν(C=S) and a band at 718 cm^{-1} to a mixture of ν(C=S) and ν(C-C). For thiourea Yamagouchi et al (62) assign bands at 1417 cm^{-1} and 1083 cm^{-1} to mixtures of NH_2 rocking, N-C-N stretching and C=S stretching, and a band at 730 cm^{-1} to C=S and N-C-N stretching.

Thioamides and thioureas are expected to be stabilized by polar resonance structures in the same way as amides and ureas. Coordination through sulfur would increase the contribution by such structures, and on this count might be expected to be more common than coordination through nitrogen.

Although the complexes formed by thioureas have been extensively studied, those of thioamides have received comparatively little attention. Flint and Goodgame (14) have prepared complexes of thioacetamide with various salts of iron II, cobalt II and nickel II. The infrared spectra suggest in all cases that coordination occurs through sulfur. Those absorption bands involving appreciable C=S stretching character, especially that at 718 cm^{-1}, are shifted to lower energy on coordination, while a band at 1393 cm^{-1} assigned as ν(C-N) in the ligand is slightly raised on coordination.

Yamagouchi et al (62) prepared complexes of thiourea with $PtCl_2$, $PdCl_2$, $ZnCl_2$ and $Ni(SCN)_2$. The band at 1417 cm^{-1} which has some C=S stretching character is lowered on coordination, while the band at 1083 cm^{-1} is extremely weak or absent. This observation is explained by the considerable change in the nature of the C-N and C=S bonds on coordination of thiourea through sulfur; the N-C-N stretching frequency is increased and the C=S stretching frequency is decreased. Therefore, the contribution of the C=S vibration to the 1083 cm^{-1} band is smaller and its intensity is reduced. The symmetric N-C-N stretching vibration (A_1) cannot contribute much to the intensity. The 730 cm^{-1} band of thiourea is found to be lowered in frequency in the complexes, again due to decreased C=S double bond character.

Swaminathan and Irving (63) have studied a fairly extensive list of thiourea complexes and conclude that coordination occurs through sulfur without exception. They base their conclusions on a splitting of the 1417 cm^{-1} ligand band, and a splitting and lowering in frequency of the 730 cm^{-1} band. They do not confirm the disappearance or weakening of the 1083 cm^{-1} band noted by Yamagouchi et al (62). It is suggested that this band is more reasonably due to NH_2 rocking than a mixture of N-C-N stretching and C=S stretching (51).

Rivest (57) suggests that in complexes with $TiCl_4$, thiourea, 1,3-diethylthiourea, 1,1-diphenylthiourea and 1,3-diphenylthiourea coordinate through nitrogen. The infrared spectra show marked decreases in the frequencies of N-H stretching bands, increased frequency of NH_2 deformation bands, and increased frequency of bands of mixed C=S and C-N stretching character. Lane et al (64) have investigated complexes of methylthiourea with $PdCl_2$, $PtCl_2$, CuCl, $ZnCl_2$ and $CdCl_2$, and conclude that in the zinc and cadmium complexes coordination occurs through sulfur whereas in the other complexes it probably occurs through nitrogen.

Magnetic Moments

The iron complexes in this study are all of high spin d^6 electronic configuration, and show paramagnetism typical of materials with incomplete electron shells. Paramagnetism arises from the spin and orbital angular momenta of these electrons. Each atomic system can be regarded as posessing a magnetic dipole of moment $\vec{\mu} = (\vec{L} + 2\vec{S})\beta$ where $\vec{L}$ is the total orbital angular momentum and $\vec{S}$ is the total spin angular momentum (in units of $h/2\pi$) of the set of electrons in the atom. The unit of magnetic moment is β, the Bohr Magneton. When a magnetic field is applied to a paramagnetic substance there is a tendency for the magnetic dipoles to line up, resulting in an induced magnetic field B inside the specimen. The induced field is related to the applied field H by

$$\vec{B} = \vec{H} + 4\pi\vec{I} \tag{26}$$

where I is the intensity of magnetization. The quantity of most chemical importance is the magnetic susceptibility χ, defined as

$$\chi = I/Hd \tag{27}$$

where d is the density of the material.

All materials posess diamagnetism for which the magnetic susceptibility is small and opposite in sign to the paramagnetic susceptibility. Diamagnetic corrections for both the metal cation and the ligands must be added to the observed susceptibility to obtain the true paramagnetic susceptibility. For the purposes of diamagnetic corrections it is convenient to deal with molar susceptibilities $\chi_M = \chi \cdot$molecular weight. A susceptibility which has been corrected for the presence of diamagnetic components is denoted by χ_M'.

The effective magnetic moment of a substance can be defined in terms of the molar susceptibility.

$$\mu_{eff} = (N\beta^2/3k)^{-1/2}(\chi_M{}'T)^{1/2} = 2.84\ (\chi_M{}'T)^{1/2} \qquad (28)$$

where N is Avogadro's Number, β is the Bohr Magneton, k is Boltzmann's constant and T is the absolute temperature.

The quantum mechanical description of the magnetic moment, in the absence of spin-orbit coupling, is

$$\mu_{eff} = \sqrt{L(L+1) + 4S(S+1)}\ \beta \qquad (29)$$

where L and S are the total orbital and spin angular momenta respectively. Spin-orbit coupling is small in first row transition metals and can usually be neglected. For an iron II nucleus placed in an octahedral ligand field the d-orbitals split into a lower triply degenerate t_{2g} set and an upper doubly degenerate e_g set. In a tetrahedral field these sets are reversed in energy. In the weak field (spin free) case, the d-electron configurations will be $t_{2g}{}^4 e_g{}^2$ for an octahedral complex and $e^3 t_2{}^3$ for a tetrahedral complex. In either case the values of L and S are both 2. The expected magnetic moment is about 5.6β. However, orbital angular momentum is often partially or fully quenched in such cases. For an electron to have orbital angular momentum about an axis it must be possible to transform the orbital which it occupies into an exactly equivalent and degenerate orbital by a rotation about the axis in question. For example, in a free ion, a rotation about the z-axis of 45° transforms the $d_{x^2-y^2}$ orbital into the d_{xy} orbital and gives to the ion an orbital angular momentum of ± 2 (in units of $h/2\pi$) about the z-axis.

Similarly, transformation of the d_{xz} orbital into the d_{yz} orbital on rotation through 90° contributes ±1 unit. The d_{z^2} orbital does not contribute to the orbital angular momentum about this axis.

But the presence of a ligand field upsets this rotation mechanism. For example, in both tetrahedral and octahedral fields the equivalence of the $d_{x^2-y^2}$ and d_{xy} orbitals is destroyed, so that their contribution of 2 units of angular momentum no longer occurs. In general, predictions of orbital contribution to the magnetic moment in tetrahedral and octahedral complexes may be made as follows. Firstly, since e_g orbital members cannot be transformed into each other by a rotation about any axis, an electron occupying them cannot contribute to the orbital angular momentum. Secondly, when there is an electron in each of the three t_{2g} orbitals, all with the same spin, the electron in the d_{xz} orbital, say, cannot rotate into the equivalent orbital d_{yz} because that orbital is already occupied. Hence the configuration t_{2g}^3 does not contribute to the orbital angular momentum.

It is seen that for high spin iron II in a tetrahedral environment, orbital angular momentum will be totally quenched and magnetic moments approaching the spin only value (Equation 30) of 4.90β will be expected.

$$\mu_{eff} = \sqrt{4S(S + 1)}\ \beta \qquad (30)$$

Octahedral complexes, however, should retain some orbital angular momentum. This will become quenched if significant distortion from octahedral symmetry destroys the degeneracy of the d_{xz} and d_{yz} orbitals, or shifts their energy significantly above the lowest lying d-orbital. The latter would be expected to occur in the case of axial distortion in which the d-levels

approach the configuration expected for a square planar complex, shown below.

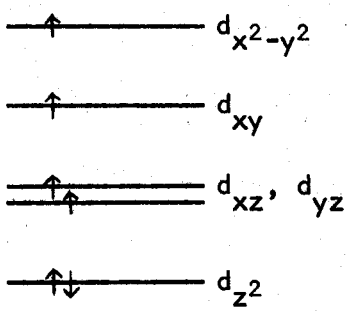

In such a case any orbital contribution which did occur would be expected to be strongly temperature dependent.

CHAPTER II

Experimental

Preparative Methods

(1) Amide, Urea and Aniline Complexes

The complexes $FeCl_2(FA)_2$, $FeCl_2(FA)_4$, $FeCl_2(MFA)_2$, $FeCl_2(DMFA)_2$, $FeCl_2(AM)_2$, $FeCl_2(BUA)_3$, $FeCl_2(BM)$, $FeCl_2(AN)$, $FeCl_2(MU)_6$ and $FeCl_2(DMU)_3$* were all prepared according to the method of Singh and Rivest (18). In this method, organic ligands react with iron pentacarbonyl (or other iron carbonyls) in the presence of halogenated hydrocarbons. These workers investigated the reaction in the presence of dichlorodiphenylmethane and suggested the following mechanism:

$$Fe(CO)_5 + 2L = Fe(CO)_3L_2 + 2CO$$

$$2Fe(CO)_3L_2 + 2(C_6H_5)_2CCl_2 = 2FeCl_2L_2 + (C_6H_5)_2C{=}C(C_6H_5)_2 + 6CO$$

In the present work the halogenated hydrocarbon was chloroform. No special precautions were taken to exclude air during the reaction other than the initial deoxygenation of the chloroform. It appears that the CO liberated is sufficient to maintain a non-oxidizing atmosphere over the reaction. Triiron dodecacarbonyl is a satisfactory substitute for iron pentacarbonyl in all the preparations which use this reagent. Further manipulations such as filtering and washing of products and preparation of samples were done under nitrogen in a dry box.

---

*FA = formamide; AM = acetamide; MFA = N-methylformamide; DMFA = N,N-dimethylformamide; BUA = isobutyramide; BM = benzamide; AN = aniline; MU = N-methylurea; DMU = N,N'-dimethylurea.

The method of Singh and Rivest was unsatisfactory for the preparation of $FeCl_2(UREA)_2$ due to insolubility of urea in chloroform and in the preparation of $FeBr_2(DMU)_3$ and $FeBr_2(AN)_3$ due to halogen exchange with the chloroform. Alternative methods for the preparation of these three complexes and also for $FeCl_2(FA)_4$, $FeCl_2(MU)_6$ and $FeCl_2(DMU)_3$ are described.

Preparations of complexes with N-methylacetamide, N-phenylacetamide, N,N'-diphenylurea and tetramethylurea were also attempted, but only oxidized products were obtained. Drago et al (65) have studied the electronic spectra of a series of complexes $[Ni(AMIDE)_6](ClO_4)_2$ and have established an order of M-O interaction based on Dq values obtained. they find a sharp break between amides in which R_1 and R_3 are both alkyl groups and amides in which one or both of R_1 and R_3 are hydrogen. (See diagram below.) The former group shows smaller M-O interaction, and this is attributed to the steric repulsion which must be present in these complexes.

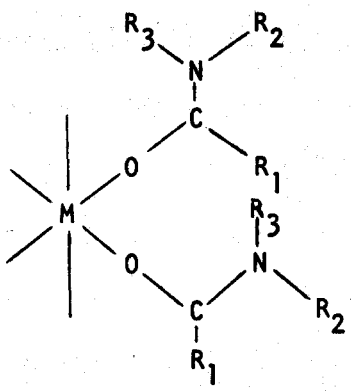

(This explanation would also apply to polymeric octahedral chlorine bridged complexes in which the amides occupy axial positions.) The instability of iron II complexes with the above named ligands could well be due to similar effects.

Dichlorobisformamideiron II - 6 gm iron pentacarbonyl and 3.5 gm formamide were refluxed in 100 ml chloroform for one week. The white powder obtained was filtered, washed with chloroform and dried in vacuo. A chlorine analysis and Mossbauer spectrum showed that this product was a mixture of $FeCl_2(FA)_2$ and $FeCl_2(FA)_4$. The mixture was dissolved in absolute ethanol, and the solution poured into 100 ml absolute ether. A white powder immediately precipitated, and was filtered, washed with ether and dried in vacuo. This product was pure $FeCl_2(FA)_2$. (Found: Cl, 31.50%. Theoretical for $FeCl_2(FA)_2$: Cl, 32.70%)

Dichlorotetrakisformamideiron II - 6 gm iron pentacarbonyl and 6 gm formamide were refluxed in 100 ml chloroform for one week. A good yield of colorless crystals was obtained, along with some unreacted formamide. The crystals were washed quickly with absolute ethanol so as to remove excess formamide but not dissolve the crystals. They were further washed with chloroform and dried in vacuo. (Found: Fe, 18.10%; Cl, 23.19%. Theoretical for $FeCl_2(FA)_4$: Fe, 18.21%; Cl, 23.10%)

An alternative preparation is as follows. A solution of 1.5 gm anhydrous ferrous chloride in 10 ml absolute ethanol was shaken with powdered iron until green. It was centrifuged and the supernatant liquid poured into 2 gm formamide. White crystals gradually formed and were filtered, washed with chloroform and dried in vacuo. (Found: Cl, 23.50%)

Dichlorobis-N-methylformamideironII - 6 gm iron pentacarbonyl and 7.5 gm N-methylformamide were refluxed in 100 ml chloroform for 24 hours. A small yield of cream colored crystals was obtained and was filtered,

washed with chloroform and dried in vacuo. (Found: Fe, 23.30%; Cl,29.48%. Theoretical for $FeCl_2(MFA)_2$: Fe, 23.00%; Cl, 29.20%)

Dichlorobis-N,N-dimethylformamideiron II - 6 gm iron pentacarbonyl and 6 gm N,N-dimethylformamide were refluxed in 100 ml chloroform for one week. A fair yield of white crystals was obtained and was filtered, washed with chloroform and dried in vacuo. More product was obtained by pouring the filtrate into an equal volume of absolute ether and allowing the mixture to stand for five days. White crystals gradually formed and were filtered, washed with chloroform and dried in vacuo. (Found: Cl, 23.42%. Theoretical for $FeCl_2(DMFA)_2$: Cl, 25.99%)

Dichlorobisacetamideiron II - 6 gm iron pentacarbonyl and 4.5 gm acetamide were refluxed in 100 ml. chloroform for one week. The white crystals obtained were washed with chloroform and dried in vacuo. (Found: Fe, 22.60%; Cl, 28.95%. Theoretical for $FeCl_2(AM)_2$: Fe, 22.80%; Cl, 28.96%)

Dichlorotrisisobutyramideiron II - 6 gm iron pentacarbonyl and 5.5 gm isobutyramide were refluxed in 100 ml chloroform for two days. The colorless crystals obtained were washed with chloroform and dried in vacuo. (Found: Fe, 14.51%; Cl, 19.03%. Theoretical for $FeCl_2(BUA)_3$: Fe, 14.39%; Cl, 18.28%)

Dichloromonobenzamideiron II - 6 gm iron pentacarbonyl and 3.6 gm benzamide were refluxed in 100 ml chloroform for 24 hours. The spongy white precipitate obtained was washed with chloroform and dried in vacuo. (Found: Fe, 21.30%; Cl, 26.72%; C, 33.25%; H, 2.48%; N, 5.55%. Theoretical for

$FeCl_2(BM)$: Fe, 22.55%; Cl, 28.61%; C, 32.92%; H, 2.85%; N, 5.65%)

Dichlorohexakis-N-methylureairon II - 6 gm iron pentacarbonyl and 5.5 gm N-methylurea were refluxed in 100 ml chloroform for four days. A small amount of white crystalline product was obtained along with unreacted N-methylurea which crystallized out as the flask cooled. The mixture was thoroughly washed with acetone to redissolve the excess N-methylurea, then dried in vacuo. (Found: Fe, 9.56%; Cl, 11.95%. Theoretical for $FeCl_2(MU)_6$: Fe, 9.78%; Cl, 12.42%)

An alternative preparation is the following. A solution of 1.5 gm anhydrous ferrous chloride in 10 ml acetone was shaken with powdered iron until green. It was centrifuged, and the supernatant liquid poured into 5 gm N-methylurea dissolved in acetone. A fine pale yellow powder precipitated immediately and was filtered, washed with acetone and fried in vacuo. (Found: Fe, 10.20%; Cl, 12.32%)

Dichlorotris-N,N'-dimethylureairon II - 6 gm iron pentacarbonyl and 5.4 gm N,N'-dimethylurea were refluxed in 100 ml chloroform for 20 hours. The colourless crystal platelets obtained were washed with chloroform and dried in vacuo. (Found: Fe, 14.35%; Cl, 18.07%; C, 27.52%; H, 6.22%; N, 21.27%. Theoretical for $FeCl_2(DMU)_3$: Fe, 14.29%; Cl, 18.14%; C, 27.68%; H, 6.19%; N, 21.50%)

An alternative method of preparation is as follows. A solution of 1.5 gm anhydrous ferrous chloride in 10 ml acetone was shaken with powdered iron until green. It was centrifuged, and the supernatant liquid poured into a solution of 3 gm N,N'-dimethylurea in acetone. The mixture was poured into 100 ml absolute ether. A white powder precipitated

which was filtered, washed with chloroform and dried in vacuo. (Found: Fe, 14.10%; Cl, 17.89%)

Dibromotris-N,N'-dimethylureairon II - A solution of 1.25 gm ferrous bromide in 10 ml acetone was shaken with powdered iron until green. It was centrifuged, and the supernatant liquid poured into a solution of 2 gm N,N'-dimethylurea in acetone. A buff colored precipitate separated gradually, which was filtered, washed with acetone and dried in vacuo. (Found: Fe, 11.77%; Br, 33.58%. Theoretical for $FeBr_2(DMU)_3$: Fe, 11.64%; Br, 33.30%)

Dichlorobisureairon II - A solution of 1.5 gm ferrous chloride in 10 ml absolute ethanol was shaken with powdered iron until green. It was centrifuged, and the supernatant liquid poured into a solution of 2 gm urea in ethanol. A tan coloured precipitate formed in about two hours and was filtered, washed with ether and dried in vacuo. (Found: Fe, 21.50%; Cl, 28.50%. Theoretical for $FeCl_2(UREA)_2$: Fe, 22.62%; Cl, 28.73%)

Dichloromonoanilineiron II - 2 gm triiron dodecacarbonyl and 1.2 gm aniline were refluxed in 100 ml chloroform for 30 hours. A fine yellow powder formed which was filtered, washed with chloroform and dried in vacuo. (Found: Cl, 32.82%. Theoretical for $FeCl_2(AN)$: C., 32.25%)

Dibromotrisanilineiron II - A solution of 1.25 gm ferrous bromide in 20 ml absolute ethanol was shaken with powdered iron until green. It was filtered into 2.5 gm aniline. A pale green precipitate formed which was filtered, washed with cold ethanol and dried in vacuo. (Found: Fe, 11.66%. Theoretical for $FeBr_2(AN)_3$: Fe; 11.29%)

(2) Thioacetamide, Thiourea and Benzothiazole Complexes

Dichloro- and dibromobisthioacetamideiron II - A solution of 0.015 moles of the anhydrous ferrous halide in 10 ml acetone was shaken with powdered iron until green. It was centrifuged, and the supernatant liquid poured into a solution of 3 gm thioacetamide in acetone. The mixture was poured into 100 ml chloroform. Pale green crystals separated out gradually and were filtered, washed with acetone and dried in vacuo. (Found for $FeCl_2(THA)_2$: Fe, 20.00%; S, 23.05%. Theoretical: Fe, 20.65%; S, 23.15%. Found for $FeBr_2(THA)_2$: Fe, 15.20%; S, 17.05%. Theoretical: Fe, 15.28%; S, 17.54%)

Dichlorobis- and dichlorotetrakisthioureairon II - A solution of 1.5 gm ferrous chloride in 10 ml absolute ethanol was shaken with powdered iron until green, centrifuged, and the supernatant liquid poured into a solution of 3 gm thiourea in ethanol. On cooling in an ice bath, pale green cubic crystals formed which were filtered, washed with ethanol and dried in vacuo. (Found: Fe, 12.60%; S, 29.80%. Theoretical for $FeCl_2(THU)_4$: Fe, 12.96%; S, 29.75%) The supernatant liquid from the first product was poured into about 200 ml chloroform. A pale green powder precipitated which was filtered, washed with chloroform and dried in vacuo. (Found: Fe, 19.38%; S, 22.90%. Theoretical for $FeCl_2(THU)_2$: Fe, 20.02%; S, 23.00%)

Dichlorobis-N-methylthioureairon II - A solution of 1.5 gm ferrous chloride in 10 ml ethanol was shaken with powdered iron until green, centrifuged, and the liquid poured into a solution of 3 gm N-methylthiourea in ethanol.

A small yield of silvery grey crystals formed overnight and were filtered, washed with ethanol and dried in vacuo. (Found: Fe, 18.39%; S, 19.08%. Theoretical for $FeCl_2(MTHU)_2$: Fe, 18.20%; S, 20.90%)

Dichlorobis-N,N'-dimethylthioureairon II - A solution of 1.5 gm ferrous chloride in 10 ml ethanol was shaken with powdered iron, centrifuged, and the supernatant liquid poured into a solution of 3 gm N,N'-dimethylthiourea in ethanol. A pale blue-green powder precipitated immediately and was filtered, washed with ethanol and dried in vacuo. (Found: Fe, 16.20%; S, 17.70%. Theoretical for $FeCl_2(DMTHU)_2$: Fe, 16.69%; S, 19.15%)

Dichloro- and dibromobisbenzothiazoleiron II - A solution of the ferrous halide in ethanol was set aside over iron powder overnight, then filtered into a slight excess over the calculated amount of benzothiazole. The complexes precipitated almost immediately. They were filtered, washed with ethanol and dried in vacuo. (Found for $FeCl_2(BTH)_2$: Fe, 13.73%; Cl, 18.80%; S, 14.48%. Theoretical: Fe, 14.07%; Cl, 17.87%; S, 16.16%. Found for $FeBr_2(BTH)_2$: Fe, 11.16%; Br, 33.80%. Theoretical: Fe, 11.49%; Br, 32.90%)

Preparations of iron II complexes with thiobenzamide, N,N'-diphenylthiourea, dimethyldiphenylthiourea and tetramethylurea were also attempted. Products were either unobtainable or oxidized. An explanation for the instability of complexes with bulky ligands has already been suggested (p. 45).

Materials

All solvents were reagent grade and were dried and deoxygenated before use. Chloroform was distilled from phosphorus pentoxide. Iron pentacarbonyl and triiron dodecacarbonyl were obtained from Alfa Inorganics and were used without further purification. All ligands were reagent grade and were used without further purification. Formamide, acetamide, thioacetamide and thiourea were obtained from Fisher Scientific Company; urea, benzamide, N-methylformamide and N,N'-dimethylformamide from Eastern Chemical Corporation; isobutyramide, N,N'-dimethylurea and benzothiazole from Eastman Organic Chemicals; N-methylurea from Baker Chemical Company; N,N'-dimethylthiourea from Aldrich Chemical Company; and N-methylthiourea from K & K Laboratories.

Chemical Analyses

Chlorine was analyzed as silver chloride by precipitation with silver nitrate and back titration with potassium thiocyanate (66). Iron was determined gravimetrically as ferric oxide after precipitation as ferric hydroxide (66). Sulfur was determined as barium sulfate after precipitation with barium chloride (66). Carbon, hydrogen and nitrogen analyses were done by the Gygli Microanalysis Laboratory in Toronto.

Mossbauer Spectra

Mossbauer spectra were recorded with an Austin Science Associates model S3 drive system, used in conjunction with a Victoreen PIP400 A multichannel analyzer operating in multiscalar mode. The power supply was an ORTEC 401A Modular System Bin. The gamma source was ^{57}Co in a palladium matrix, obtained from the New England Nuclear Corporation. The strength of the source was roughly 5 millicuries. The 14.4 KeV gamma ray was detected in the initial stages of the work by a thin (1/32") NaI(Tl) activated crystal with matching photomultiplier tube, type "SHG", manufactured by the Harshaw Chemical Company. This detector was operated at 1275 volts. In the later stages of the work a gas filled proportional counter, model CSP-400, manufactured by Austin Science Associates, was used. The fill gas was Xe-CO_2 at one atm. pressure. Operating voltage was 2000 volts. This detector unit included a close coupled field effect transistor preamplifier. Power for the detector units was supplied by a DC regulated power supply, model 2K-10, from Power Designs Pacific, Inc.

The elements of the Mossbauer spectrometer are indicated in a block diagram in Fig. 7. The source is moved to and fro with constant acceleration. The velocity, and hence the gamma ray energy, varies linearly with time and has a triangular waveform as shown in Fig. 8. The velocity waveform is monitored on an oscilloscope. The Mossbauer spectrum consists of a plot of count rate vs velocity. The 400 channels in the analyzer cover one drive cycle of increasing and decreasing source velocity. As a result, two mirror image spectra are obtained, with one being counted during intervals of increasing velocity and the other during intervals of decreasing velocity.(Fig. 8).

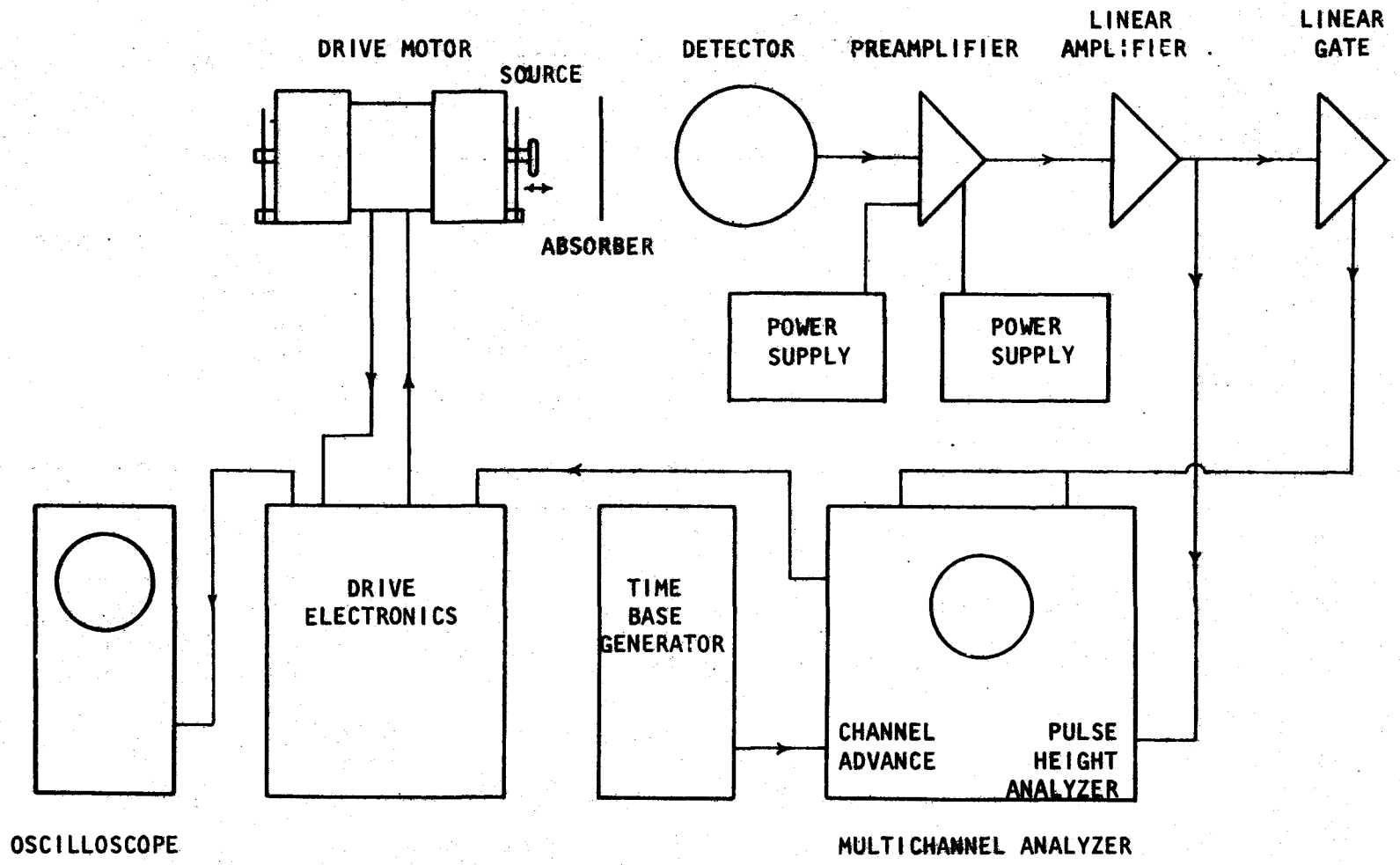

Figure 7. Block diagram of Mossbauer Spectrometer.

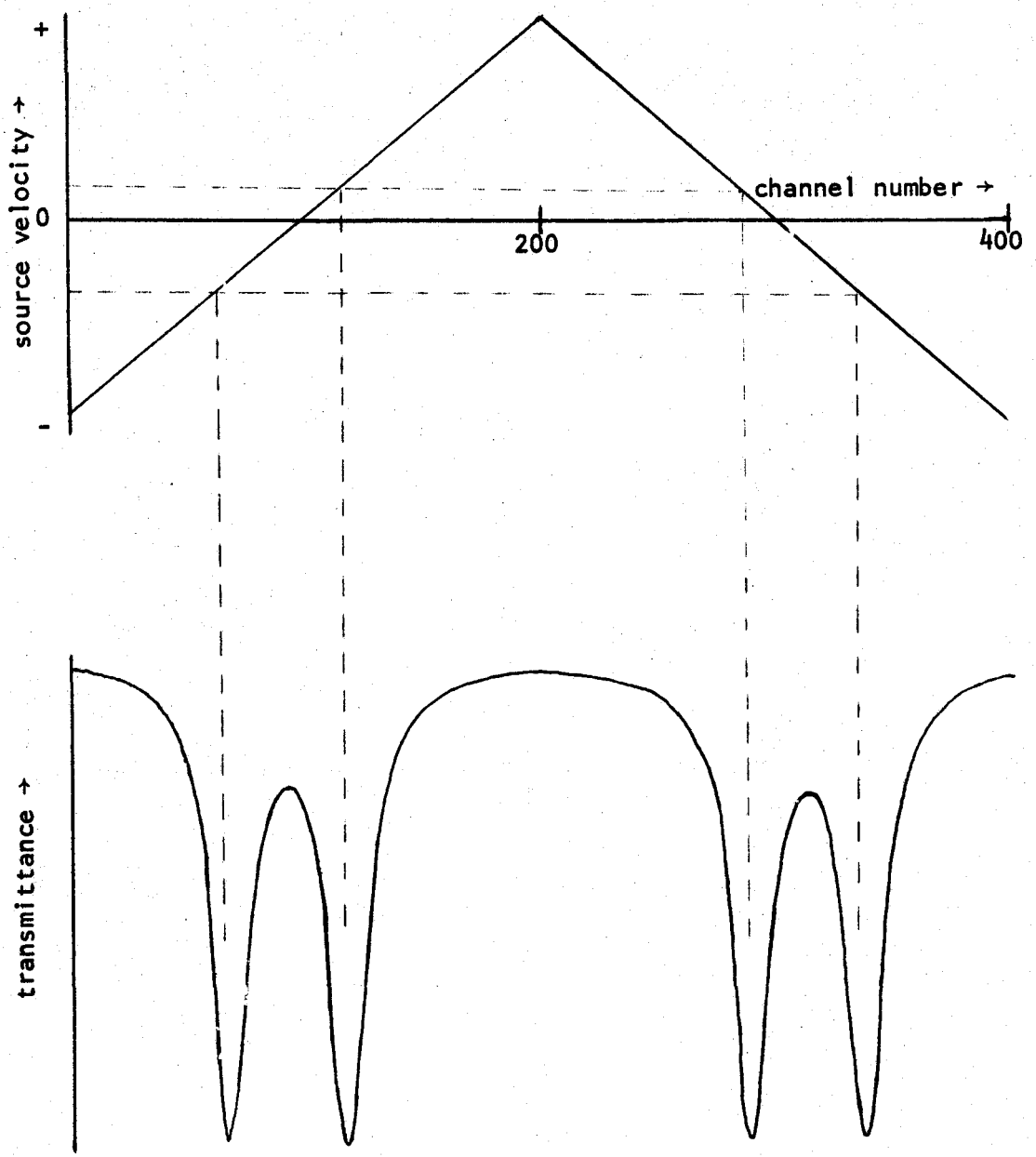

Figure 8. Source velocity waveform and mirror image Mossbauer spectra counted during intervals of increasing and decreasing velocity.

There typically several energies of gamma and X-rays emitted by the source. It is essential that an energy selective detector be used, so that only the desired gamma rays will be counted. The pre-amplifier and a linear amplifier amplify and shape the resulting pulses. Voltage levels may be adjusted in the single channel analyzer to further select the 14.4 KeV gamma ray. The signal from the single channel analyzer is then counted by the multichannel analyzer, whose channel address varies in synchronism with the source velocity. A crystal controlled time base generator provides the signals for address advance. The velocity drive is controlled by a signal from the multichannel analyzer.

Spectra with baselines of approximately 50,000 counts accumulated in one to six hours using the proportional counter, depending on sample concentration of iron, presence of other heavy gamma absorbing nuclei and temperature. Spectra counted with the NaI scintillation detector accumulated in roughly twice the time required with the proportional counter.

Spectra were recorded at 295°K and 77°K. The cooling system for the low temperature spectra, which employed a thermistor controlled automatic topping device for the liquid nitrogen dewar, is shown in Fig. 9.

Treatment of Mossbauer Data

Spectra were printed out as counts per channel on a Teletype paper tape punch. The information was transferred to cards, and peaks were fitted to Lorentzian line shapes using an iterative least squares method.

The velocity scale was calibrated with a sodium nitroprusside absorber. All isomer shifts are quoted with respect to the centroid of the sodium nitroprusside spectrum, and quadrupole splittings with respect to

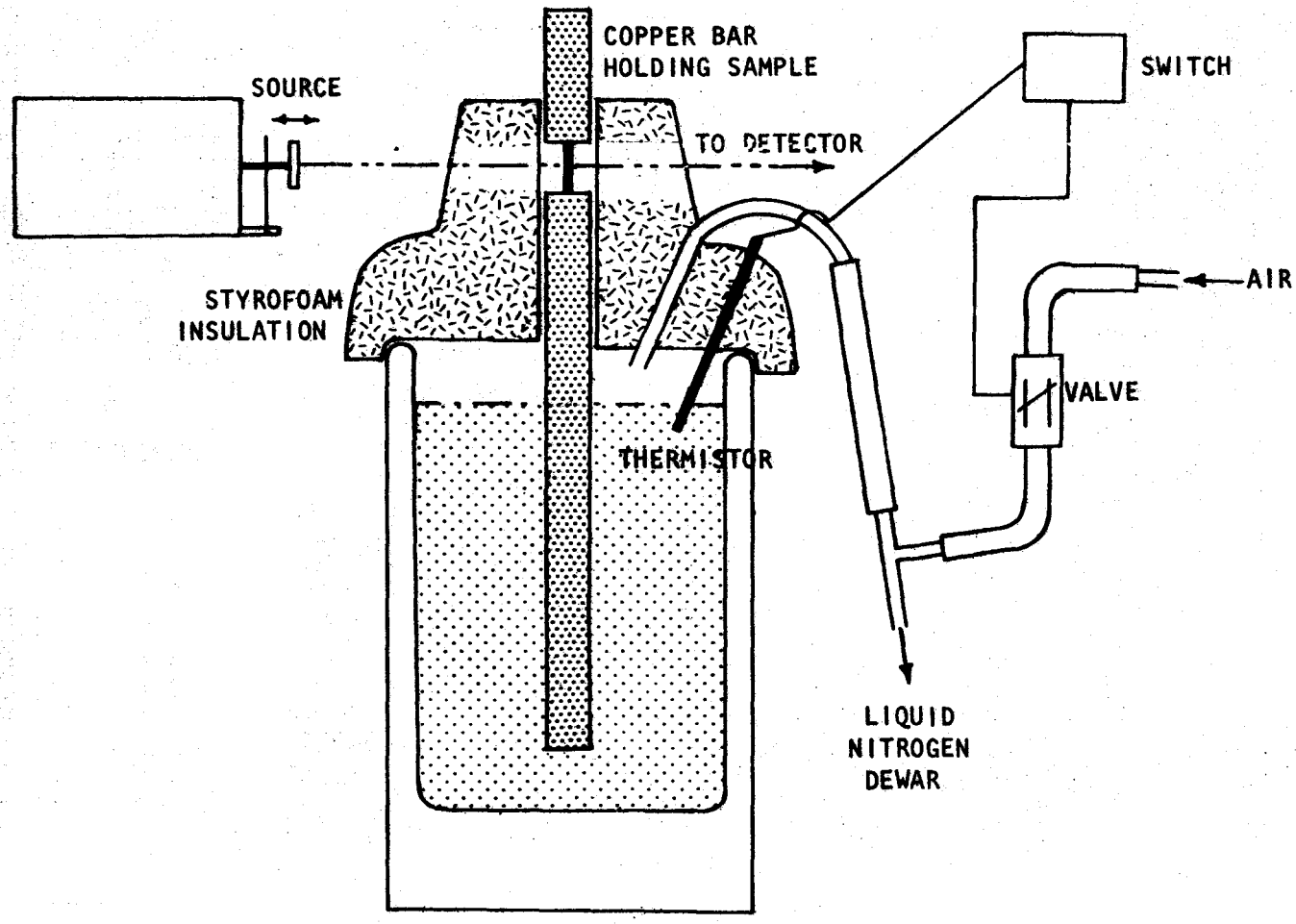

Figure 9. Cooling system for Mossbauer sample.

the sodium nitroprusside quadrupole splitting of 1.712 mm/sec. Isomer shifts are thought to be accurate to ±0.02 mm/sec and quadrupole splittings to ±0.05 mm/sec. These deviations have been estimated by comparing the parameters calculated from the left and right hand sides of the Mossbauer spectra.

Samples generally contained 10 to 15 mg/cm^2 of iron. Complexes containing bromine were found to be strongly gamma absorbing and consequently showed very low count rates and small peak intensities. They were diluted to as little as 6 mg/cm^2 of iron in order to increase the count rate and observe significant intensity in the Mossbauer peaks. Because of these varying sample concentrations comparisons of spectral intensities between different samples are not valid. Some qualitative correlations will nevertheless be made in the next chapter.

Infrared Spectra

Infrared spectra in the region 4000 to 400 cm^{-1} were recorded on a Perkin Elmer 521 Grating Infrared Spectrophotometer. Solid samples of ligands and complexes were recorded an nujol or fluorolube mulls between KBr windows. Liquid samples of ligands and solutions of ligands in dioxane were also recorded between KBr windows in a normal infrared cell. Dioxane was chosen as a solvent for two reasons. Firstly, it is thought to have little or no hydrogen bonding characteristics, and so should give N-H and C=O stretches of ligands in solution which are unshifted by hydrogen bonding. Secondly, dioxane is sufficiently viscous and non-volatile that it can be used in a normal infrared cell rather than a liquid cell. Reagent grade dioxane was obtained from Fisher Scientific Company and used without further purification.

Far infrared spectra in the region 400 to 200 cm^{-1} were recorded as nujol mulls between polyethylene windows on a Beckman IR 12 instrument.

Magnetic Measurements

Magnetic susceptibilities were measured by the Gouy balance method on equipment described already (67).

CHAPTER III

Results and Discussion

Benzothiazole Complexes

It will be convenient to introduce this chapter with a discussion of the benzothiazole complexes. Dichlorobisbenzothiazoleiron II and dibromobisbenzothiazoleiron II have been found exemplary of the Mossbauer and far infrared spectra expected for octahedral and tetrahedral iron complexes respectively. They will provide a basis for interpretation of much of the subsequent data.

The electronic spectra of the iron II benzothiazole complexes have been reported previously and structural assignments made (3). The complex $FeCl_2(BTH)_2$ had an electronic spectrum typical of a polymeric octahedral iron II complex (Fig. 10A). Two low intensity bands were observed at 9050 and 6600 cm^{-1} and were similar to those found for $FeCl_2(py)_2$ (py = pyridine), which has this polymeric structure (68). They were assigned as transitions between the split components of the ^5Eg state. The complex $FeBr_2(BTH)_2$ gave an entirely different electronic spectrum, with intense absorption at low energy (6330 cm^{-1}) and a series of weak bands, or shoulders, at higher energy. This is typical of iron II complexes in a tetrahedral environment (Fig. 10B), the intense absorption being due to the $^5E \rightarrow {}^5T_2$ transition. Similar electronic spectra have been observed for complexes FeX_2L_2 (X = Cl, Br; L = quinoline, 3-methylisoquinoline) and by analogy these are also thought to be monomeric tetrahedral species (13).

Figure 10.

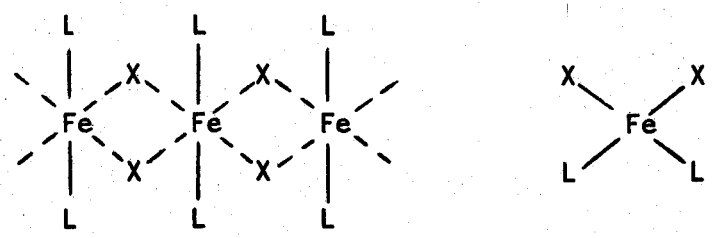

A B

Mossbauer Spectra

The Mossbauer data for the benzothiazole complexes are given in Table III. The isomer shift of the bromo complex is about 0.3 mm/sec less positive than that for the chloro complex. Some of this difference may arise from different covalent character in Fe-Br and Fe-Cl bonds, but this effect is thought to be minor (36). A more satisfactory explanation is that the chloro complex, being 6-coordinate, is significantly less covalent than the bromo complex which is 4-coordinate. Indeed, the isomer shifts of 1.36 and 1.05 mm/sec for these complexes fit nicely into the expected ranges for 6-coordinate and 4-coordinate iron II respectively (p. 21). The Mossbauer spectra are shown in Fig. 11.

Table III. Mossbauer Data for the Benzothiazole Complexes

Complex	Temperature	IS(mm/sec)	QS(mm/sec)	Absorption(%)* Low Vel.	High Vel.
$FeCl_2(BTH)_2$	295°K	1.36	1.46	10.0	9.0
	77°K	1.49	1.76	19.8	17.5
$FeBr_2(BTH)_2$	295°K	1.05	2.82	1.3	1.3
	77°K	1.17	3.02	2.9	3.5

*Uncorrected values (p. 58)

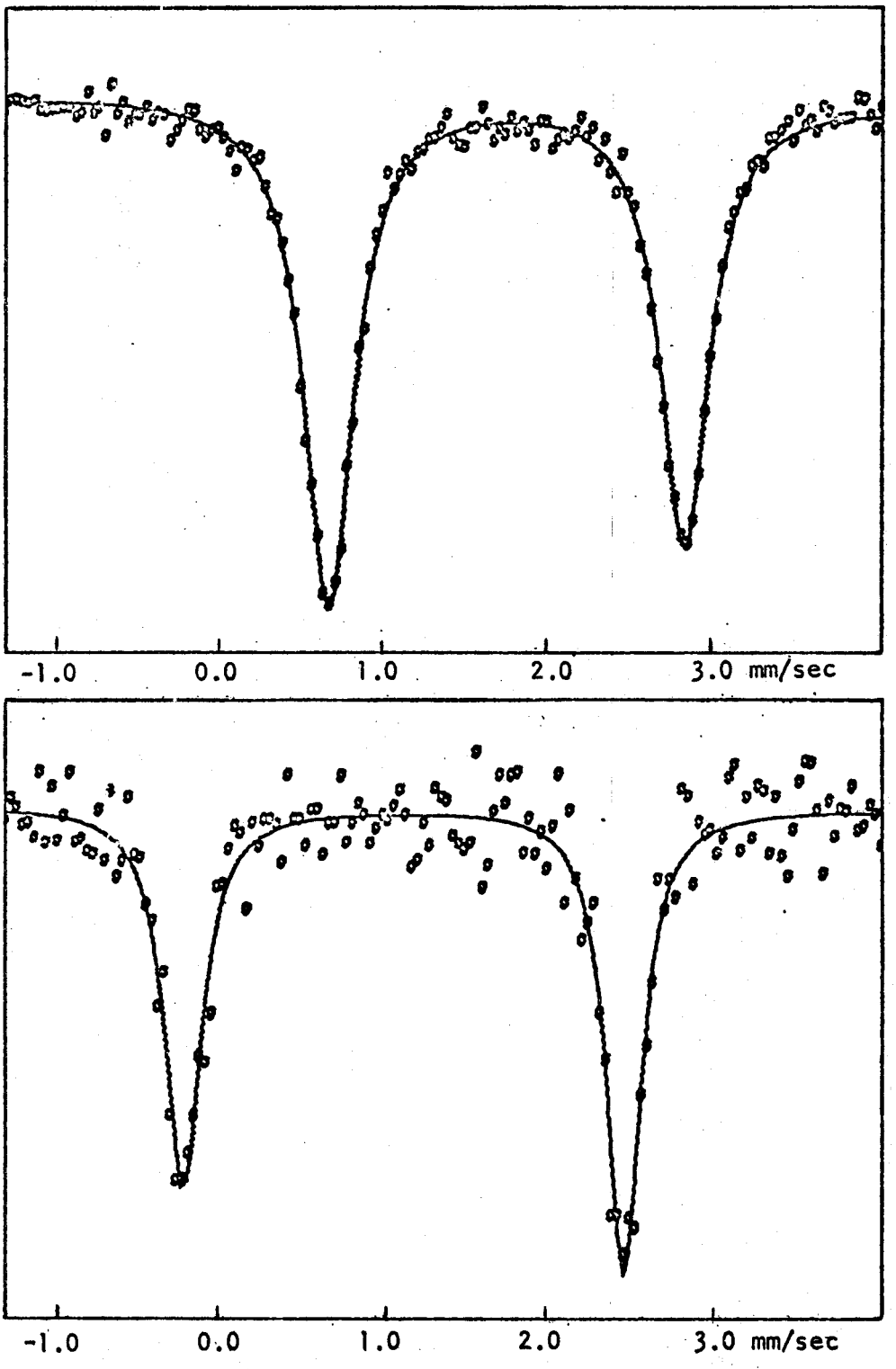

Figure 11. Mossbauer spectra of $FeCl_2(BTH)_2$ (top) and $FeBr_2(BTH)_2$ (bottom) at 77°K.

The quadrupole splittings for the two benzothiazole complexes do not follow the trend which might be predicted on the basis of covalency effects. Increased bond covalency in the bromo complex due to small coordination number and capacity of the bromide ion to form covalent bonds should result in a decreased quadrupole splitting. In this case the determining factors may be steric. If the benzothiazole ligand is bulky enough that the axial Fe-L bonds are longer than the bridged chlorine bonds in the xy plane then the axial ligand field may be sufficiently weak for the complex to have a d_{xz} or d_{yz} ground state. Quadrupole splittings associated with these ground states are only about half as large as those associated with a d_{xy}, $d_{x^2-y^2}$ or d_{z^2} ground state due to the smaller electric field gradient contribution from the d_{xz} and d_{yz} orbitals (eq. 23-25). This explanation could account for the octahedral chloro complex having a much smaller quadrupole splitting than the tetrahedral bromo complex.

An estimation of the distortional splitting in the e levels using equation 23 gives $\Delta \simeq 750\ cm^{-1}$ for the bromo complex. When deviations of 0.05 mm/sec in the quadrupole splitting data are taken into account, Δ values calculated from equation 23 are at best accurate to within about $20\ cm^{-1}$. Δ values greater than $700\ cm^{-1}$ can only be approximately assigned by this method because of the very large errors introduced by only a small error in the quadrupole splittings.

Substitution of $\Delta = 750\ cm^{-1}$ back into equation 23 gives an extrapolated QS_{max} (quadrupole splitting at 0°K) of 3.03 mm/sec. $FeSiF_6 \cdot 6H_2O$ gives a value of 3.79 mm/sec. at 4.2°K (69). This is the highest known value for a ferrous compound. The lattice terms have been calculated to be small (70), and for the high trigonal distortion

involved, the spin-orbit and rhombic terms will also be small. If $FeSiF_6 \cdot 6H_2O$ is assumed to be a free ion case this implies that $FeBr_2(BTH)_2$ has an α^2 value of at most about 80%, but 65% would seem more reasonable.

The spectral intensities of the benzothiazole complexes illustrate two expected trends in iron Mossbauer spectra. Firstly, a very weak absorption is observed for the bromo complex at room temperature whereas the chloro complex absorbs relatively strongly at this temperature. (However, see p. 58). Other workers (5, 9, 19) have found tetrahedral compounds of iron to exhibit weak or undetectable absorption at room temperature. Secondly, the temperature dependence of the intensity is noticeable greater for the bromo complex than for the chloro complex. Both these observations suggest a lower Debye temperature for the bromo complex than for the chloro complex. This is expected in view of the proposed structures of these species.

Infrared Spectra

The far infrared bands of the benzothiazole complexes are given in Table IV. The two Fe-Br stretches assigned for the bromo complex are strong and well resolved, and are typical of tetrahedral complexes MBr_2L_2 (Table II). In the spectrum of the chloro complex there are at least two

Table IV. Far Infrared Bands for the Benzothiazole Complexes

Complex	ν(Fe-X)	ν(Fe-L)	Ligand Bands
$FeCl_2(BTH)_2$	(251 m, 197 s)		363 m
$FeBr_2(BTH)_2$	266 s, 244 s	205 m	363 m

poorly resolved bands which have not been assigned. However, the absence of any Fe-Cl stretching vibration above 250 cm^{-1} is evidence in favor of a polymeric octahedral chlorine bridged structure (p. 33). The spectra are shown in Fig. 12.

An infrared study of the benzothiazole complexes in the 400 - 4000 cm^{-1} region was not made due to the complex nature of the spectrum of benzothiazole. It was anticipated that identification of the coordinating atom from peak shifts in this region would have been unreliable. Chan et al (3) suggest that in the complexes $Co(BTH)_2(ClO_4)_2$ and $Ni(BTH)_2I_2$ coordination of benzothiazole occurs through nitrogen rather than sulfur. They base their suggestion on the similarity of the electronic spectra of these complexes to those of the analogous benzimidazole complexes where the coordination must be through nitrogen.

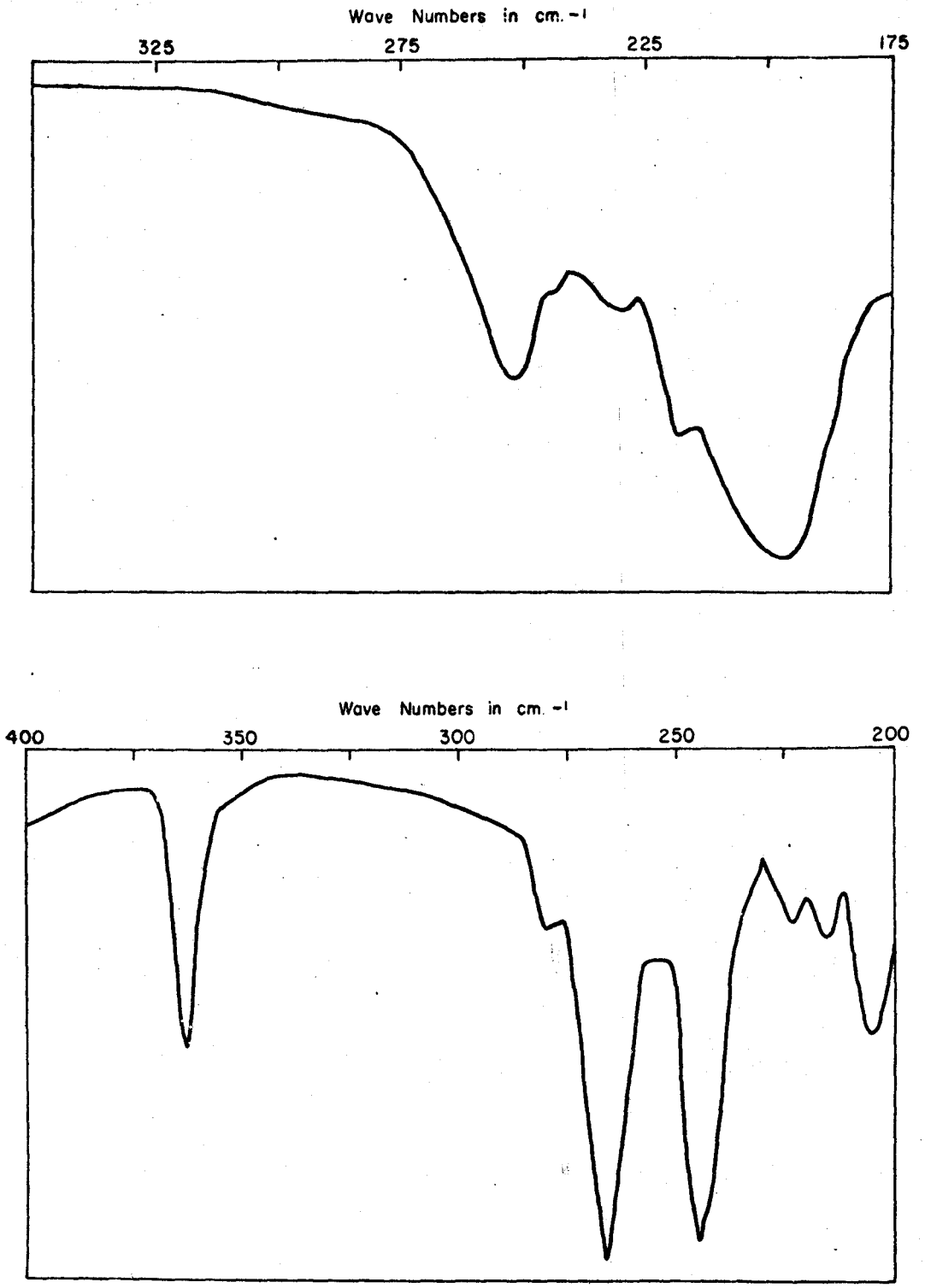

Figure 12. Far infrared spectra of $FeCl_2(BTH)_2$ (top), and $FeBr_2(BTH)_2$ (bottom).

Thioacetamide and Thiourea Complexes

Complexes of thioacetamide, thiourea, N-methylthiourea and N,N'-dimethylthiourea with ferrous chloride and of thioacetamide and thiourea with ferrous bromide have been prepared. In all cases complexes of stoichiometry FeX_2L_2 were formed. The Mossbauer, infrared and magnetic data support assignment of tetrahedral structures to these complexes. In addition, a 1:4 complex $FeCl_2(THU)_4$ was prepared which will be shown to be octahedral.

Mossbauer Spectra

The Mossbauer data for the thioacetamide and thiourea complexes are given in Table V. The isomer shifts for the 1:2 complexes all fall in the region expected for 4-coordinate iron II, while that for the 1:4 complex is noticeably more positive and in the range expected for 6-coordinate iron II. Substitution of bromide for chloride appears to have no detectable effect on the isomer shift, supporting a similar observation by Duncan et al (36). The quadrupole splittings are all greater than 3 mm/sec, suggesting that the structures are considerably distorted from cubic symmetry. Also, the temperature dependence of the quadrupole splittings is slight. An estimation of the distortional splittings in the e_g levels using equation 23 gives $\Delta \simeq 800$ cm^{-1} in all the tetrahedral cases. Such highly distorted structures may result from the difference in covalency of Fe-X and Fe-S bonds; the ligands under discussion are shown to be coordinated through sulfur by means of infrared spectral data. Substitution of $\Delta = 800$ cm^{-1} back into equation 23 gives extrapolated QS_{max} values of 3.3 to 3.5 mm/sec, and α^2 values somewhat larger than for $FeBr_2(BTH)_2$.

Table V. Mossbauer Data for the Thioacetamide and Thiourea Complexes

Complex	Temperature	IS(mm/sec)	QS(mm/sec)	Absorption(%)* Low Vel.	High Vel.
$FeCl_2(THA)_2$	295°K	0.97	3.15	6.0	4.0
	77°K	1.09	3.28	17.5	14.0
$FeBr_2(THA)_2$	77°K	1.07	3.49	1.7	1.3
$FeCl_2(THU)_2$	295°K	1.00	3.26	1.0	1.0
	77°K	1.10	3.41	3.4	4.2
$FeBr_2(THU)_2$	295°K	0.99	3.32	1.3	1.9
	77°K	1.09	3.45	3.7	4.8
$FeCl_2(MTHU)_2$	295°K	0.98	3.23	4.1	4.1
	77°K	1.11	3.33	12.6	12.2
$FeCl_2(DMTHU)_2$	295°K	1.01	3.29	3.8	3.6
	77°K	1.11	3.41	10.5	8.6
$FeCl_2(THU)_4$	295°K	1.27	3.46	4.0	4.0
	77°K	1.40	3.56	7.2	7.2

*Uncorrected values (p.58)

This would indicate a slightly greater covalency in $FeBr_2(BTH)_2$, but isomer shift values show an opposite relationship. However, as mentioned previously, the derivation of Δ values from equation 23 leads to large errors when Δ is large and these values must be considered very approximate.

The magnitude of the quadrupole splitting of the 1:4 thiourea complex requires that it have a d_{xy} ground state. A comparison of its temperature dependence, namely an increase of only 0.1 mm/sec between room temperature and 77°K, with Fig. 6 in chapter I suggests a distortional

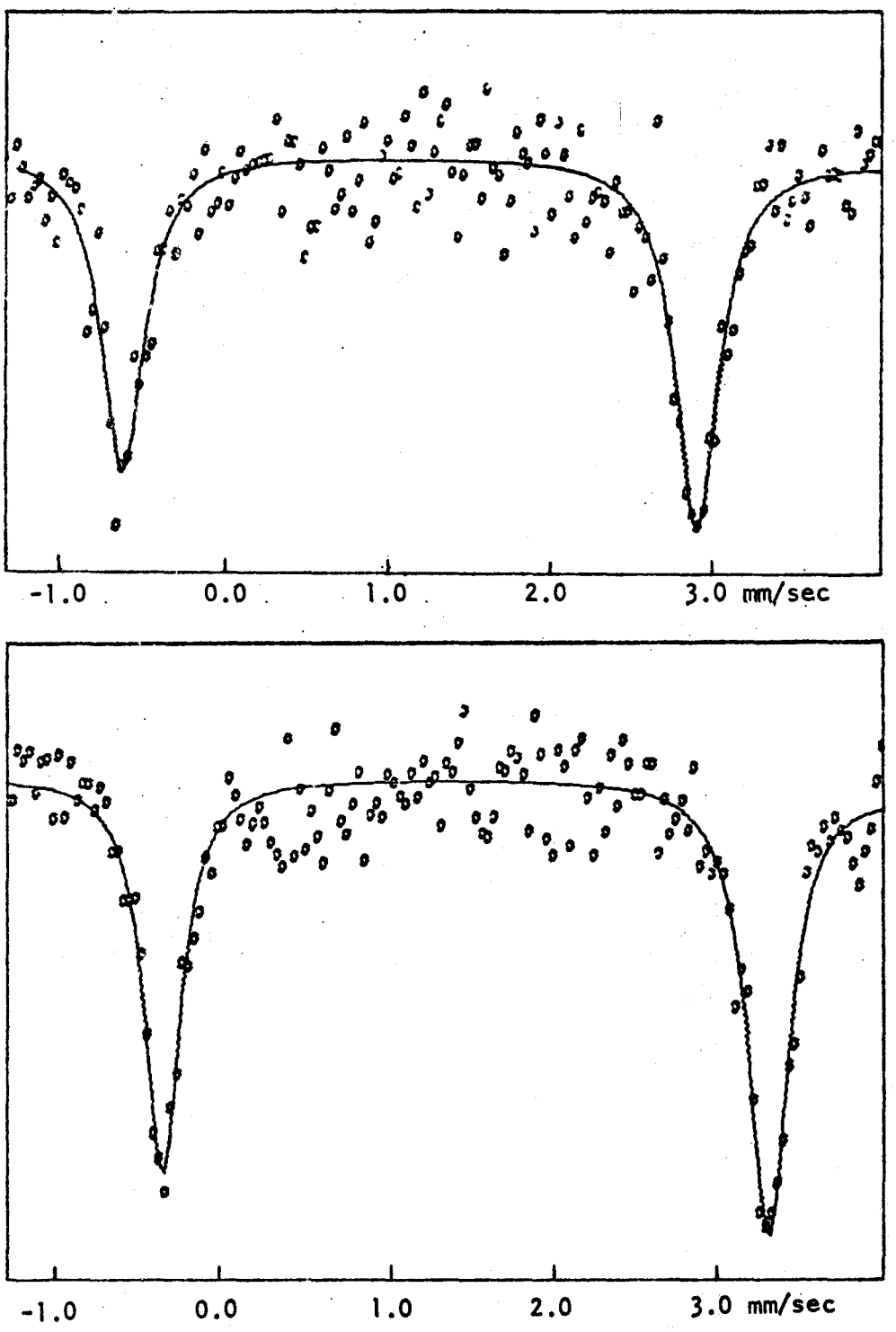

Figure 13. Mossbauer spectra of $FeCl_2(THU)_2$ (top) and $FeCl_2(THU)_4$ (bottom) at 77°K.

splitting of $\Delta \simeq 1000\ cm^{-1}$ in the t_{2g} levels. Spin-orbit effects in such a highly distorted structure will be small. The Mossbauer spectra of the 1:2 and 1:4 thiourea complexes are shown in Fig. 13.

The room temperature absorption in the Mossbauer spectra of the 1:2 complexes is in most cases very small. However, since the intensities are not corrected for varying sample concentrations of iron, presence of heavy gamma absorbing nuclei such as bromine, etc., comparisons of intensities between different samples is not strictly valid (p.58). The temperature dependence of the intensity is noticeably greater for the 1:2 complexes than for the 1:4 thiourea complex, suggesting a lower Debye temperature for the former and giving further support to assignment of tetrahedral structures.

Infrared Spectra

The far infrared bands of the thioacetamide and thiourea complexes are listed in Table VI. Assignments have been made in some cases.

Table VI. Far Infrared Bands of the Thioacetamide and Thiourea Complexes

Complex	ν(Fe-X)	ν(Fe-L)	Ligand Bands
$FeCl_2(THA)_2$	328 s, 304 s	235 s	385 w
$FeBr_2(THA)_2$	(260 sh, 253 s, 238 m, 235 sh)		387 w
$FeCl_2(THU)_2$	315 s, 293 s	248 s	—
$FeBr_2(THU)_2$	(270 w, 240 w, 212 m)		—
$FeCl_2(MTHU)_2$	325 sh, 300 vs	255 m	—
$FeCl_2(DMTHU)_2$	305 vs	278 m	—
$FeCl_2(THU)_4$	(227 m, 202 m)		—

That $FeCl_2(THA)_2$ and $FeCl_2(THU)_2$ are clearly tetrahedral species is seen by the occurrence of two ν(Fe-Cl) stretches in the 300 cm^{-1} region (Table II). The analogous bromides presumably have similar structures but their far infrared spectra are not so well resolved and are not readily assignable. It has been suggested in the case of $FeBr_2(THA)_2$ that the bands in this region are strongly coupled ν(Fe-Br) and ν(Fe-S) vibrations (14). The methylthiourea and dimethylthiourea complexes have infrared spectra which are noticeably different from those of $FeCl_2(THA)_2$ and $FeCl_2(THU)_2$ (Fig. 14). Both show a very strong, well resolved peak at about 300 cm^{-1} and a less intense absorption to lower frequency. These have been tentatively assigned as ν(Fe-Cl) and ν(Fe-S) respectively. Iron-chlorine stretching in the 300 cm^{-1} region again supports the tetrahedral structures of these complexes. No explanation is advanced to account for the occurrence of only one ν(Fe-Cl) band in the 300 cm^{-1} region instead of the expected two.

The 1:4 thiourea complex shows two bands at low frequency. The number and positions of the bands support assignment of a trans octahedral structure to this complex (Table I). Both the ν(Fe-Cl) and ν(Fe-S) vibrations are expected to be decreased in frequency due to longer, weaker bonds in the octahedral complex. The shift in Fe-Cl stretching in the 1:2 and 1:4 thiourea complexes may be compared with the shift noted by Clark (43) in Co-Cl stretching in 1:2 and 1:4 pyridine complexes. In the tetrahedral species two ν(Co-Cl) bands occur at 344 cm^{-1} and 304 cm^{-1} and in the octahedral species one ν(Co-Cl) band occurs at 230 cm^{-1}.

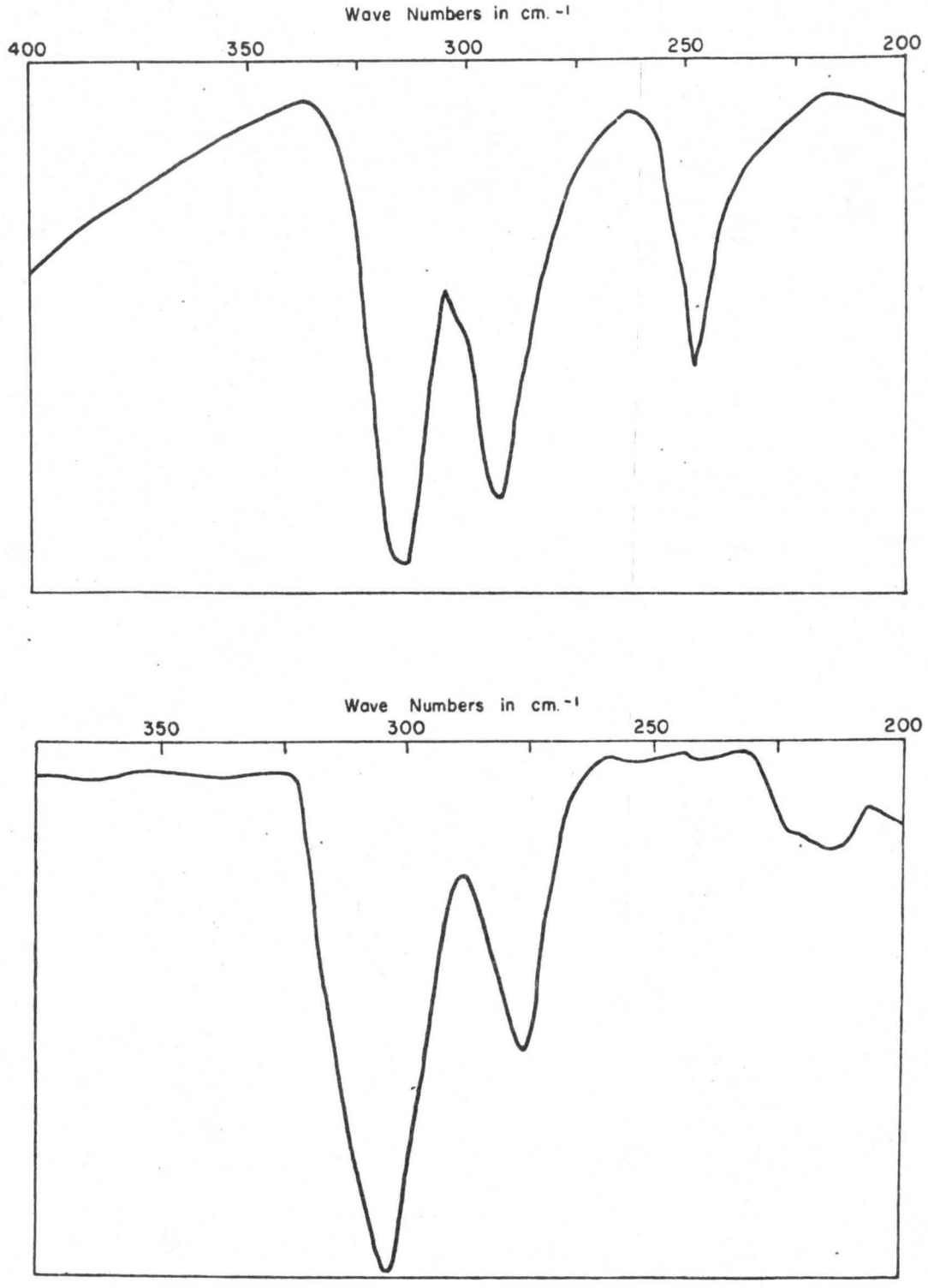

Figure 14. Far infrared spectra of $FeCl_2(THU)_2$ (top), and $FeCl_2(DMTHU)_2$ (bottom).

Table VII shows the infrared spectra of thioacetamide and its complexes with $FeCl_2$ and $FeBr_2$ in the 400-4000 cm^{-1} region. Infrared bands obtained by Flint and Goodgame (14) for the complex $CoCl_2(THA)_2$ have been included for comparison. These workers suggest that thioacetamide is coordinated through sulfur in the cobalt complex. The spectra of the iron complexes are very similar to that of the cobalt complex, again supporting coordination through sulfur. In the N-H stretching region the iron complexes absorb at higher frequency than the ligand, in mull form, but at somewhat lower frequency than the ligand in dioxane solution. This suggests that there is considerably less hydrogen bonding present in the coordinated ligand than in the pure ligand, but that the NH_2 group is still not as free as in solutions of the ligand. As Singh and Rivest (18) have suggested in the case of amide complexes, some hydrogen bonding may be present in the complex between the NH_2 hydrogens and the halide. In neither of the iron complexes are there low lying N-H stretching bands which might result from coordination through nitrogen. The C-N stretching band at 1386 cm^{-1} is shifted to higher frequencies, as expected on coordination through sulfur (p. 38). The bands at 973 and 719 cm^{-1}, which are of C=S stretching character, are shifted significantly to lower frequencies on formation of S→M bonds.

Infrared spectra of the thiourea complexes are shown in Table VIII. The diagnostic regions again are the N-H stretching region and the bands of C-N and C=S stretching character. Bands in the ν(N-H) region are at significantly higher frequencies in the complexes than in the pure ligand. The absence of low lying absorption in this region again precludes the presence of N→M bonds. The N-C-N stretching band at 1472 cm^{-1} is found at higher frequencies in the complexes. The 1409 cm^{-1} band is split,

Table VII. Infrared Spectra, 400-4000 cm^{-1}, of Thioacetamide and its Complexes.

Assignment*	THA 0.2 M in dioxane	THA mull	$FeCl_2(THA)_2$ mull	$FeBr_2(THA)_2$ mull	$CoCl_2(THA)_2$** mull
ν(N-H)	3377 s	—	—	—	—
	3325 s	—	3324 s	3328 s	—
	3211 s	3280 s	3300 sh	3296 sh	—
	—	3072 s	3204 s	3196 s	—
$\delta(NH_2)$	1640 s	1648 s	1660 s	1649 s	1657
	—	—	1634 m	1632 m	1638
$\delta_a(CH_3)$	—	1479 s	1483 m	1480 m	1475
ν(C-N)	1390 m	1386 s	1407 w	1407 m	1401
$\delta_s(CH_3)$	—	1363 s	1364 m	1364 m	1362
skeletal + $\rho(NH_2)$	1311 vs	1303 vs	1292 s	1285 s	1292
$\rho(NH_2)$ + $\rho(CH_3)$	—	1031 m	1022 vw	—	1026
ν(C-C) + $\rho(CH_3)$ + ν(C=S)	981 s	973 vs	960 m	958 m	960
ν(C=S) + ν(C-C)	723 s	719 s	686 s	685 s	691
$\omega(NH_2)$ + $\tau(NH_2)$	—	709 s	729 sh	730 s	732
	—	—	716 s	712 s	—
π(C-C)	—	517 m	512 m	510 m	514
δ(NCS)	—	473 s	451 w	450 w	448
	—	461 m	442 s	442 s	—
δ(C-C)	—	378 m	385 m	387 m	395

ν = stretch; δ = deformation; ρ = rock; ω = wag; τ = twist; π = out-of-plane bend

*Reference 61.

**Reference 14.

Table VIII. Infrared Spectra, 400-4000 cm^{-1}, of Thiourea and its Complexes.

Assignment*	THU mull	$FeCl_2(THU)_2$ mull	$FeCl_2(THU)_4$ mull	$FeBr_2(THU)_2$ mull
ν(N-H)	—	3450 sh	3458 m	3450 sh
	3364 s	3395 s	3380 s	3425 s
	3356 s	3305 s	3320 sh	3378 s
	—	—	3274 s	3325 sh
	3145 s	3213 s	3184 s	3298 s
	3094 sh	—	—	3210 s
	—	—	—	3188 sh
$\delta(NH_2)$	1605 s	1625 s	1628 m	1636 s
	—	1613 s	1602 s	1618 s
ν(C-N)	1472 s	1502 w	1483 s	1518 mw
	—	1485 w	—	1495 mw
ν(C=S)	1409 s	1425 m	1439 m	1440 m
	—	1387 m	1386 s	1406 m
$\rho(NH_2)$	1072 s	1095 vw	1090 m	1110 vw
ν(C-N)	730 s	722 m	719 s	714 w
	—	703 m	706 s	704 m
skeletal	632 m	560 m	588 sh	618 w
	624 m	—	570 s	564 m
δ(C-N)	488 s	505 m	507 s	464 s
	—	464 m	469 m	—
$\tau(NH_2)$	412 m	—	426 s	—
	—	—	412 s	—

*Reference 62.

presumably into a band of predominantly C-S stretching character appearing at lower frequency and one of predominantly N-C-N stretching character at higher frequency. The band at 730 cm^{-1}, which is largely of ν(C=S) character, is both split and lower in frequency. These effects have been noted by Swaminathan and Irving (63) in other thiourea complexes and are associated with coordination through sulfur.

Tables IX and X show the infrared bands of N-methylthiourea, N,N'-dimethylthiourea and their complexes with $FeCl_2$. In neither of these complexes is there any significant shift to lower frequency of the bands in the ν(N-H) region. The dimethylthiourea complex shows only one strong N-H stretching band, supporting the presence of only one kind of nitrogen. The bands of mixed N-H bending and C-N stretching character at about 1550 cm^{-1} are shifted 20-25 cm^{-1} to higher frequencies, as are the bands of mixed C-N and C=S stretching character near 1500 cm^{-1}. It is thought that both these effects are due to an increase in C-N double bond character in the sulfur bonded ligand. N,N'-dimethylthiourea shows another band at 1355 cm^{-1} which has been tentatively assigned as mixed C-N and C=S stretching. This peak is also shifted to higher wave number on complex formation. The bands at 774 cm^{-1} in N-methylthiourea and 727 cm^{-1} in N,N'-dimethylthiourea contain predominantly C=S stretching character, and are shifted to lower frequency on coordination. The observation that none of the N-CH_3 stretching or deformation bands are significantly shifted also indirectly supports coordination through sulfur.

Table IX. Infrared Spectra, 400-4000 cm^{-1}, of N-methylthiourea and $FeCl_2(MTHU)_2$.

Assignment*	MTHU mull	$FeCl_2(MTHU)_2$ mull
ν(N-H)	—	3406 m
	—	3397 sh
	—	3343 m
	3328 m	3331 m
	3248 s	3305 s
	3165 s	3215 m
$\delta(NH_2)$	1627 s	1624 s
δ(NH) + ν_a(C-N)	1555 s	1576 s
		1564 sh
$\rho(NH_2)$ + ν_s(C-N) + ν(C=S)	1488 w	1503 m
		1486 w
$\delta_a(CH_3)$	1450 m	1452 w
$\delta_s(CH_3)$	1405 m	1416 w
		1404 m
ν_a(C-N) + δ(NH)	1293 s	1296 m
$\rho(CH_3)$	1146 m	1156 w
	1122 m	1115 w
ν_s(C-N) + $\rho(NH_2)$ + ν(C=S)	975 m	973 w
ν(C=S) + ν_s(C-N)	774 m	760 m
$\pi(NH_2)$	720 s	719 m
		698 m

*Reference 64.

Table X. Infrared Spectra, 400-4000 cm^{-1}, of N,N'-dimethylthiourea and $FeCl_2(DMTHU)_2$

Assignment*	DMTHU mull	$FeCl_2(DMTHU)_2$ mull
ν(N-H)	3230 sh 3190 s	3306 s
δ(NH) + ν(C-N)	1572 sh 1555 s	1597 s
ν(C-N) + ν(C=S)	1520 s 1490 sh	1536 s 1478 vw
$\delta_a(CH_3)$	1453 m 1440 m	1456 w 1443 w
$\delta_s(CH_3)$	1415 w	1424 w
ν(C-N) + ν(C=S)	1355 m	1382 w
ν(C-N) + δ(NH)	1288 m 1250 sh	1304 m
$\rho(CH_3)$	1186 m	1190 w
$\nu(N-CH_3)$	1040 s 1015 m	1039 m 1020 w
ν(C-N) + ν(C=S)	727 w	717 m

*Tentative assignments made with reference to infrared spectral assignments for thiourea (62) and N-methylthiourea (64).

Magnetic Moments

The magnetic moments of some of the thioacetamide and thiourea complexes are shown in Table XI. They are all consistent with magnetic moments expected for either tetrahedral iron II or highly distorted octahedral iron II.

Table XI. Magnetic Moments of Thioacetamide and Thiourea Complexes.

Complex	Temperature	μ_{eff} (β)
$FeCl_2(THA)_2$	295°K	5.27
$FeCl_2(THU)_2$	295°K	4.89
$FeCl_2(THU)_4$	295°K	5.25
$FeCl_2(MTHU)_2$	295°K	5.17
	77°K	4.83
$FeCl_2(DMTHU)_2$	295°K	5.09
	77°K	4.79

Amide, Urea and Aniline Complexes

A number of complexes of ferrous chloride and ferrous bromide with amides and ureas have been prepared. Complexes of aniline with these salts were also prepared. These complexes have been grouped together because they are all shown to contain 6-coordinate iron.

Mossbauer Spectra

The Mossbauer data are given in Table XII. With the exception of the isobutyramide complex the isomer shifts fall in the range expected for 6-coordinate iron II (p. 21). The isobutyramide complex appears to have two different iron environments (Fig. 15). It has been formulated as $[Fe(BUA)_6^{2+}][FeCl_4^{2-}]$ and the Mossbauer spectrum interpreted as containing two quadrupole split doublets, with the high velocity lines of each doublet coinciding. It is inferred from the relative peak intensities (Table XII) that the two sites are of equal abundance. The doublet with larger isomer shift (1.62 mm/sec at 77°K) is assigned to the 6-coordinate cation. The doublet of isomer shift 1.31 mm/sec observed at 77°K is assigned to the tetrachloroferrate II anion. This value agrees well with literature values for other tetrachloroferrate II complexes. Edwards et al (9) find that at 77°K the complexes $[NMe_4]_2[FeCl_4]$ and $[NEt_4]_2[FeCl_4]$ have isomer shifts of 1.27 and 1.28 mm/sec respectively.

The isomer shift of $FeCl_4^{2-}$ is much larger than the isomer shifts (1.1 mm/sec at 77°K) observed for the tetrahedral complexes FeX_2L_2 (L = sulfur-bonded ligand) discussed in the previous section. Fe-Cl bonds would be expected to be considerably more polar than Fe-S bonds, and this would account for the difference in isomer shifts observed.

Table XII. Mossbauer Data for the Amide, Urea and Aniline Complexes

Complex	Temperature	IS(mm/sec)	QS(mm/sec)	Absorption(%)* Low Vel.	High Vel.
$FeCl_2(FA)_2$	295°K	1.43	2.66	4.0	4.0
	77°K	1.54	2.93	9.0	9.0
$FeCl_2(MFA)_2$	295°K	1.40	2.46	5.0	6.7
	77°K	1.51	2.76	9.3	11.3
$FeCl_2(DMFA)_2$	295°K	1.48	2.95	9.0	11.7
	77°K	1.59	3.20	15.5	15.8
$FeCl_2(AM)_2$**	295°K	1.39	2.64	5.4	5.4
	77°K	1.55	2.80	7.7	7.7
$FeCl_2(UREA)_2$	295°K	1.45	2.59	9.7	9.7
	77°K	1.57	2.65	15.0	15.0
$FeCl_2(FA)_4$	295°K	1.46	0.66	8.0	8.0
	77°K	1.59	1.39	14.3	14.3
$FeCl_2(BM)$	295°K	1.40	2.53	3.3]	3.3
	77°K	1.52	2.81	7.3	7.3
$FeCl_2(AN)$**	295°K	1.37	1.69	3.9	3.9
	77°K	1.49	2.18	7.1	7.1
$FeCl_2(BUA)_3$	295°K	1.51	0.88	1.0	1.0
	195°K	1.31	1.28	(2.7, 2.8, 4.8)†	
		1.54	0.82		
	77°K	1.31	2.02	(5.0, 5.0, 9.8)†	
		1.62	1.40		
$FeCl_2(DMU)_3$	295°K	1.41	2.20	2.2	3.4
	77°K	1.55	3.33	8.7	12.6
$FeCl_2(MU)_6$	295°K	1.51	1.60	2.5	2.3
	77°K	1.63	2.18	8.1	7.8
$FeBr_2(AN)_3$	295°K	1.35	1.51	2.6	2.2
	77°K	1.47	1.98	7.5	6.4
$FeBr_2(DMU)_3$	295°K	1.37	1.65	1.5	2.0
	77°K	1.48	2.09	3.9	4.4

*Uncorrected values (p. 58)

**Reference 19.

†See Fig. 15.

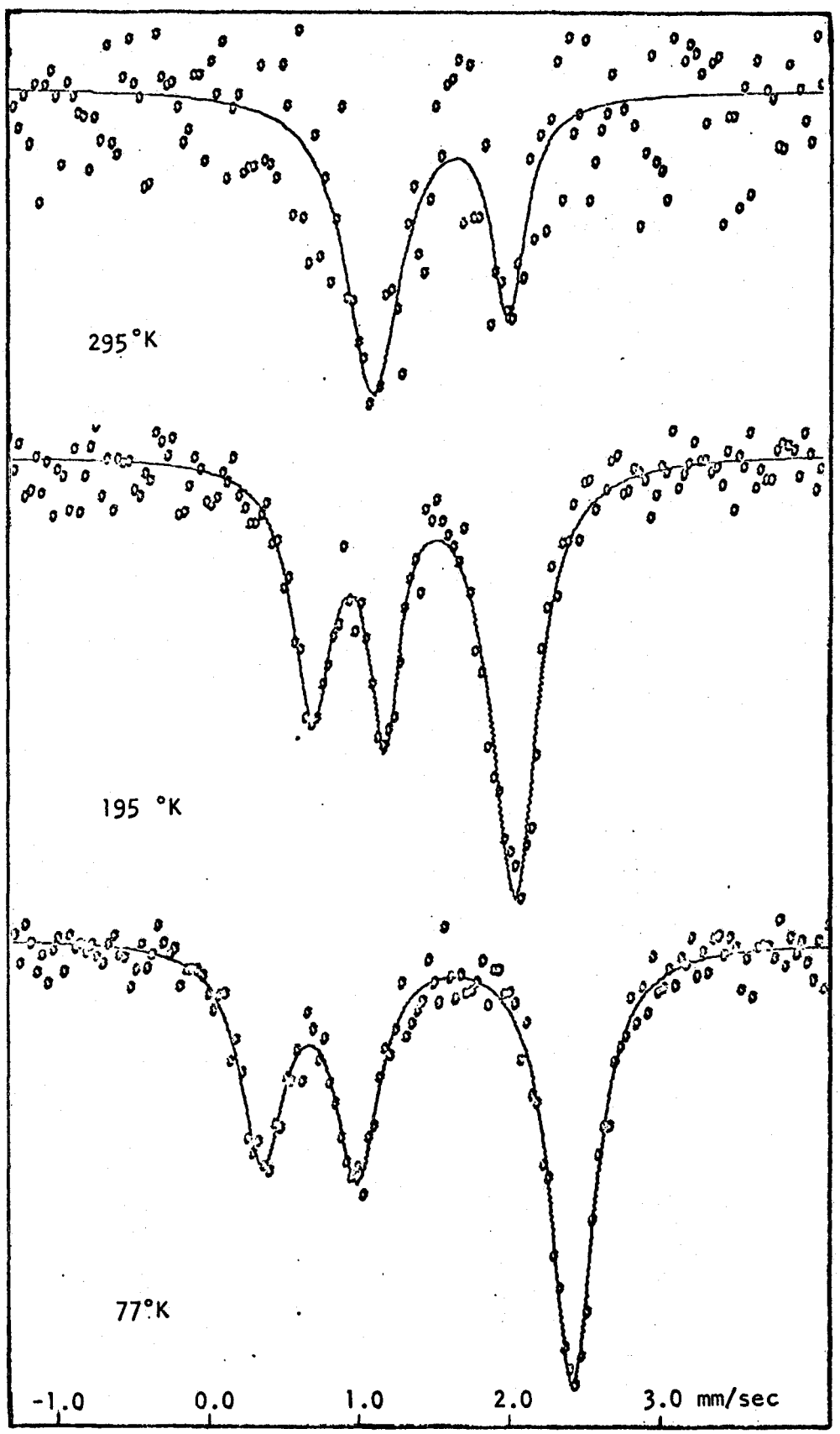

Figure 15. Mossbauer spectrum of $[Fe(BUA)_6][FeCl_4]$.

Absorption by the tetrahedral species is negligible at room temperature and explains why the spectrum apparently collapses to a doublet. Other workers (5, 9) have also found that tetrachloroferrates give very small or negligible absorption at room temperature.

The methylurea complex, like the hexaamidoferrate species in the isobutyramide complex, has an isomer shift significantly larger than the other complexes. It has been formulated as $[Fe(MU)_6]Cl_2$.

The complexes $FeCl_2L_2$ are thought to be chlorine bridged polymers like their benzothiazole analogue. Their isomer shifts fall in the region 1.40 - 1.48 mm/sec and the possibility of tetrahedral structures is hereby discounted. The 1:3 complex $FeCl_2(DMU)_3$ has been assigned a dimeric chlorine bridged structure as in Fig. 16A. The 1:1 complexes $FeCl_2(BM)$ and $FeCl_2(AN)$ are thought to form cross-linked polymers such as that in Fig. 16B. Goodgame et al (71) have proposed an analogous structure for $FeCl_2(py)$ and have interpreted its electronic spectrum on this basis. Again, the possibility of a chlorine bridged dimer containing 4-coordinate iron has been ruled out because of the magnitude of the isomer shifts.

Figure 16.

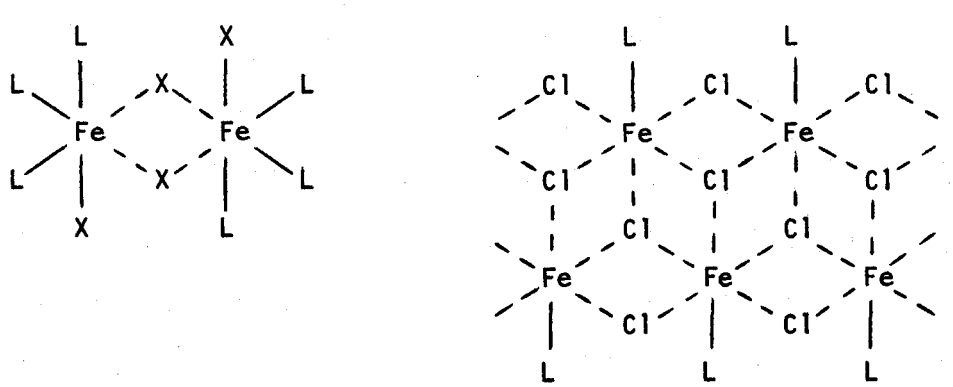

A B

Figure 17 shows a plot of isomer shift versus the number of chlorines coordinated to each iron. Allowing for the large variation in isomer shift for the $FeCl_2L_2$ complexes there does appear to be a crude correlation between isomer shift and the number of chlorine atoms in the first coordination sphere of irom. This effect has been noted previously by Edwards et al (9). These workers attribute increasing isomer shift in the series $FeCl_2$, $FeCl_2 \cdot 2H_2O$, $FeCl_2 \cdot 4H_2O$ to the greater polarizability of the chlorine ligand compared with the water ligand. This explanation applies also in the present case. It is interesting that the correlation is fairly good despite the fact that different oxygen-coordinating ligands appear in the series. The amides and ureas used are evidently very similar in their coordinating ability. The complex with N,N-dimethylformamide deviates most from the general trend, likely due to steric hindrance and possibly a longer Fe-L bond than in the other complexes. This complex was very unstable with respect to oxidation, and this also illustrates the inability of this ligand to stabilize iron II. The aniline and benzamide complexes have similar isomer shifts, illustrating the similarity in coordinating properties of this nitrogen-donor ligand to the oxygen-donor ligands.

The 1:3 bromide complexes show very similar Mossbauer spectra, and are thought to have dimeric bromine bridged structures (Fig. 16A). Their isomer shifts are about 0.5 mm/sec smaller than that of $FeCl_2(DMU)_3$, suggesting increased covalent character in the bonding. It is interesting that the effect of substituting bromide for chloride should be noticeable in this case. In the previous section substitution of bromide for chloride in the tetrahedral FeX_2L_2 complexes had a negligible effect on the isomer

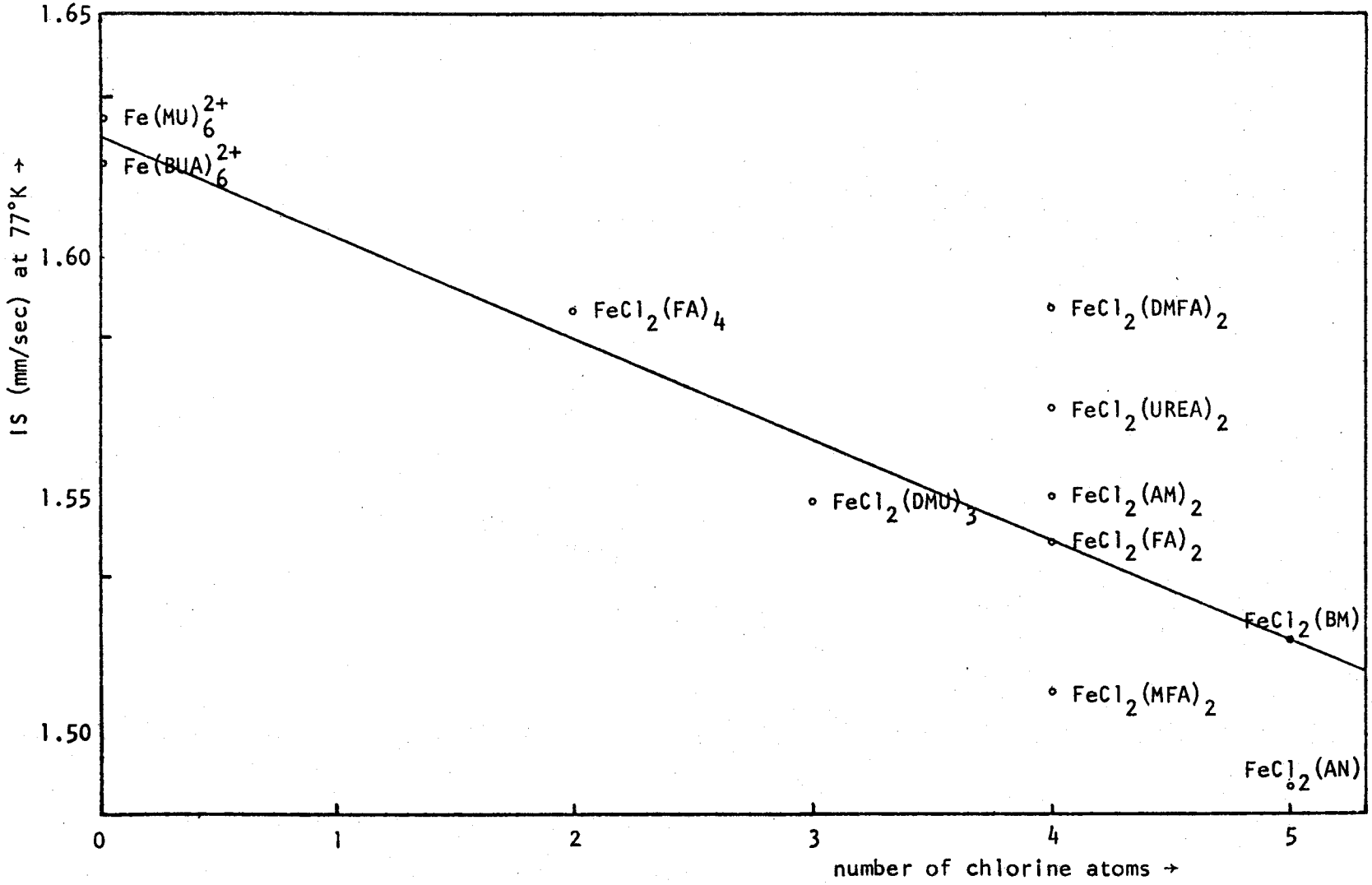

Figure 17. Isomer shift vs number of chlorine atoms in first coordination sphere of iron.

shift. Perhaps bromine has a greater ability to form bridged bonds. The Mossbauer spectra for these 1:3 complexes show no evidence for an ionic structure such as $[FeL_6^{2+}][FeX_4^{2-}]$. Only one iron site is evident even at 77°K when one would have expected to detect the presence of FeX_4^{2-}. The possibility of two exactly overlapping doublets is extremely unlikely. The isomer shift of $FeCl_2(DMU)_3$ is 1.55 mm/sec at 77°K. If $FeCl_4^{2-}$ were present it should produce a doublet with an isomer shift of about 1.31 mm/sec and this should be plainly detectable as in the case of $[Fe(BUA)]_6[FeCl_4]$. The isomer shifts of $FeBr_2(AN)_3$ and $FeBr_2(DMU)_3$ are 1.47 and 1.48 mm/sec respectively at 77°k. Again, if $FeBr_4^{2-}$ were present it should produce a doublet with isomer shift about 1.28 mm/sec (9).

The quadrupole splittings in Table XII vary considerably. All are smaller than those observed for the tetrahedral complexes of the previous section which have S-coordinated ligands. This indicates less distortion from cubic symmetry as might be expected for the complexes with O- and N-coordinated ligands. However, as pointed out in the introduction (p.29), spin-orbit effects cannot be ignored in octahedral complexes and this would also help to account for the smaller quadrupole splittings observed.

The polymeric complexes $FeCl_2L_2$ all have room temperature quadrupole splittings in the range 2.5 - 3.0 mm/sec and show small increases of 0.1 - 0.3 mm/sec at 77°K. The fact that the splittings are all greater than 2 mm/sec suggests that in these complexes, if the z-axis is the O-Fe-O axis, the d_{xy} orbital lies lowest (35). This is known to be the case for $FeCl_2 \cdot 2H_2O$. Johnson (72) has studied the Mossbauer spectrum of a single crystal of this compound at 4.2°K and 1.4°K and concludes that the direction of maximum electric field gradient is the O-Fe-O axis.

The crystal structure (73) is also in agreement, showing Fe-O bond lengths of 2.07 Å and Fe-Cl bond lengths of 2.49 Å and 2.54 Å. The observation of only a small temperature dependence in the quadrupole splittings of the $FeCl_2L_2$ complexes indicates that distortional splittings in the t_{2g} levels are of considerable size. The quadrupole splitting of $FeCl_2 \cdot 2H_2O$ shows similar behavior. Johnson (72) estimates $\Delta_1 = 520\ cm^{-1}$ and Δ_2 large with respect to the spin-orbit coupling constant of about 100 cm^{-1}.

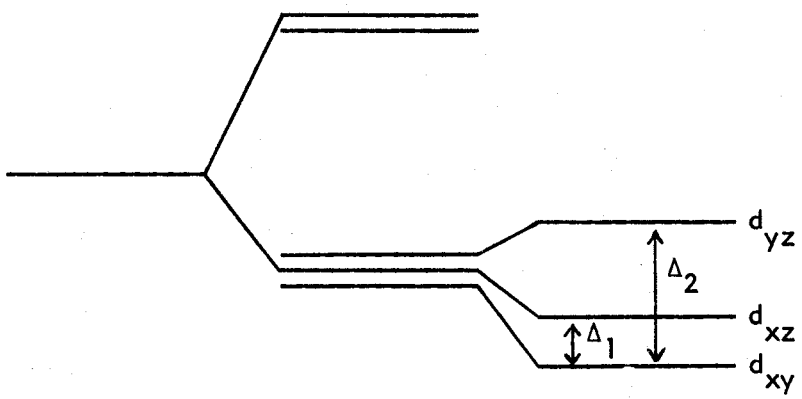

The polymeric 1:2 benzothiazole complex already discussed provides a contrast to the 1:2 O-coordinated complexes. The long Fe-L bonds are thought to produce an elongated octahedral environment in which the orbital ground state is d_{xz} or d_{yz} (p. 63). Its small quadrupole splitting (Table III) is in keeping with the prediction that iron II in such an environment gives splittings which are only half the value obtained if d_{xy} lies lowest.

The quadrupole splitting of the 1:4 formamide complex is unusually small (Fig. 18). This and the large temperature dependence point to a near octahedral structure with only small distortional splittings in the t_{2g} levels. The small value could also be due to a structure in which d_{xz} and d_{yz} lie lowest. The 1:4 thiourea complex, in contrast, is

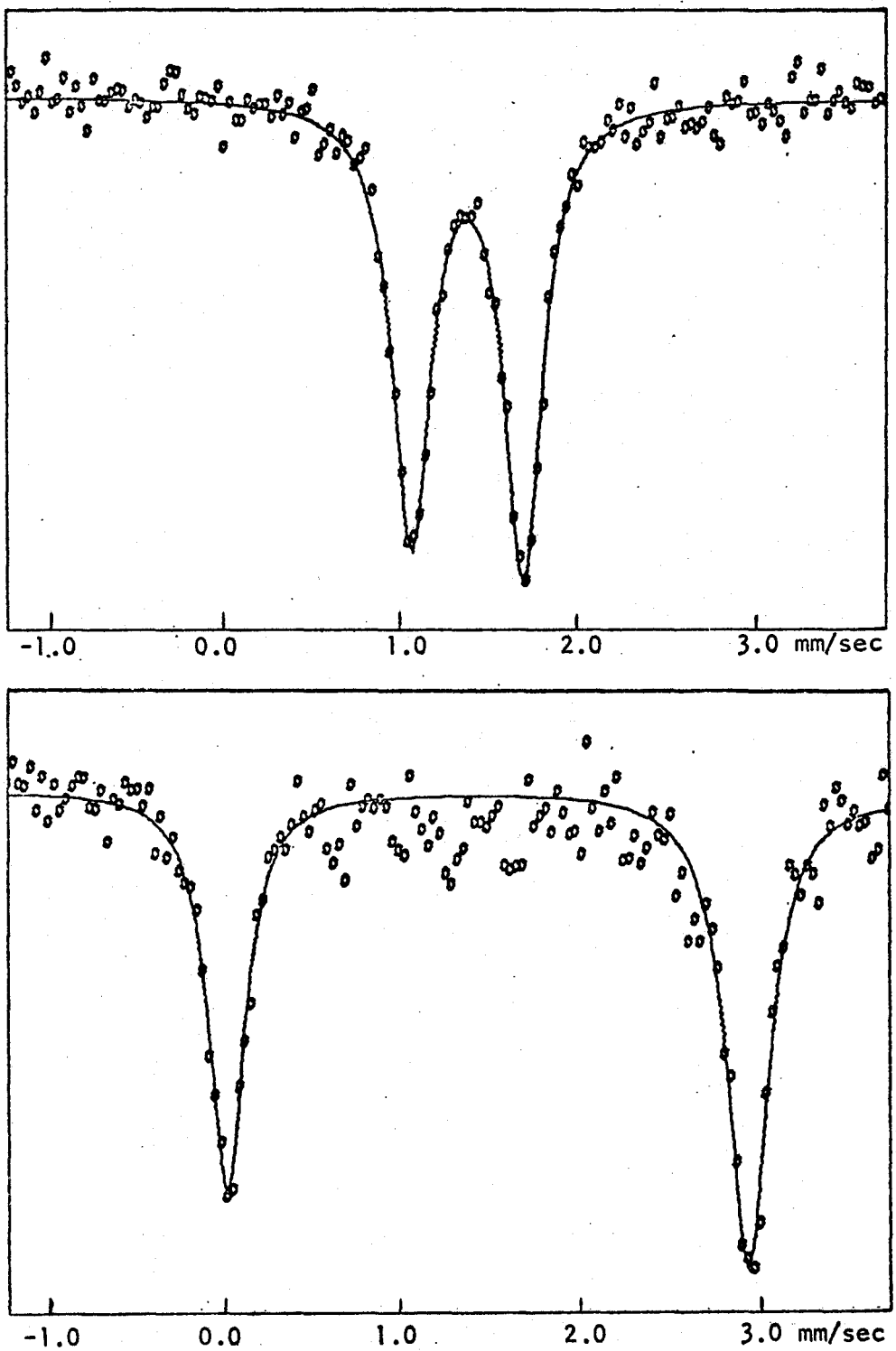

Figure 18. Mossbauer spectra of $FeCl_2(FA)_4$ (top) and $FeCl_2(DMFA)_2$ (bottom) at 295°K.

expected to have a d_{xy} ground state due to the long Fe-S bonds in the xy plane. It shows a much larger quadrupole splitting (Table V). The structure of the 1:4 formamide complex appears to differ significantly from that of $FeCl_2 \cdot 4H_2O$, for which Grant et al (74) report a room temperature quadrupole splitting of 2.98 mm/sec and almost negligible temperature dependence. The crystal structure (75) of $FeCl_2 \cdot 4H_2O$ shows it to have a distorted 6-coordinate trans structure in which Fe-Cl = 2.38 Å, Fe-O = 2.09 Å and 2.59 Å, and the angle Cl-Fe-O = 81°.

The tetrachloroferrate II anion in the isobutyramide complex shows quadrupole splittings of 1.28 and 2.02 mm/sec at 195°K and 77°K respectively. The distortional splitting in the e_g levels, as calculated from equation 23, is 185 cm^{-1}. Edwards et al (9) find similar quadrupole splittings for $[NMe_4]_2[FeCl_4]$ and $[NEt_4]_2[FeCl_4]$, and calculate Δ values of 125 cm^{-1} and 135 cm^{-1} for these complexes. Presumably the bulky $Fe(BUA)_6^{2+}$ cation produces a greater distortion than do NMe_4^+ and NEt_4^+.

The octahedral cation $Fe(BUA)_6^{2+}$ shows quadrupole splittings of 0.82 and 1.40 mm/sec at 195°K and 77°K respectively. These values indicate a near cubic environment about iron and the possibility of a doublet ground state in the d-levels. The methylurea complex, supposed to contain the octahedral cation $Fe(MU)_6^{2+}$ has somewhat larger quadrupole splittings but still within the region expected for a d_{xz} or d_{yz} ground state.

The 1:3 bromides show very similar quadrupole splittings which are smaller and less temperature dependent than those for the 1:3 chloride $FeCl_2(DMU)_3$. This may be due to a difference in d-orbital ground state or to increased covalency in Fe-Br bonds.

Infrared Spectra

The far infrared bands of the amide and urea complexes are listed in Table XIII. The similarity of the spectra of the 1:2 complexes is evident. It is proposed that all of these are 6-coordinate chlorine bridged complexes. Four bands appear in most cases, at about 180 cm^{-1}, 200 cm^{-1}, 220 cm^{-1} and 260 cm^{-1}. (The spectra of the formamide and urea complexes were not recorded below 200 cm^{-1} so that in these cases the existence of the lowest band is not certain.) The peaks are generally poorly resolved. The spectra of the acetamide and N,N'dimethylformamide complexes are shown in Fig. 19. Gill et al (68) have observed a similar far infrared spectrum for the polymeric octahedral complex $FeCl_2(py)_2$. They find three poorly resolved peaks at 238 cm^{-1}, 227 cm^{-1}, and 219 cm^{-1}.

The spectra of these 1:2 complexes are strikingly different from the tetrahedral 1:2 complexes already discussed which showed strong, well resolved Fe-Cl stretching bands close to 300 cm^{-1} (Table VI, Fig. 14). The shift of the ν(Fe-Cl) absorption region to lower frequency in the polymeric complexes is attributed to the weaker bridged chlorine bonds.

Polymeric octahedral compounds MX_2L_2 are predicted to show only three infrared active normal vibrational modes (Table I). However, deviation from axial symmetry would cause some splitting of these bands. This may account for the observation of four bands in the present cases. An alternative and perhaps more likely explanation is that one of the bands is a combination of lower deformation modes. Assignment of Fe-Cl or Fe-O stretching character to the peaks has not been attempted. It is expected that these vibrations will be strongly coupled.

Table XIII. Far Infrared Bands of the Amide and Urea Complexes.

Complex	ν(Fe-X)	Bridged ν(Fe-X)		ν(Fe-O)		Ligand Bands
$FeCl_2(FA)_2$	—	(262 s	220 m	195 s)		—
$FeCl_2(MFA)_2$	—	(251 m 245 m	222 m	204 s 196 s	170 m)	392 s 377 s
$FeCl_2(DMFA)_2$	—	(—	227 s	200 s	180 m)	390 s 377 s
$FeCl_2(AM)_2$	—	267 m	228 s	204 s	186 m 174 m	—
$FeCl_2(UREA)_2$	—	(266 s	222 s	200 s)		—
$FeCl_2(BM)$	291 m	(252 m	225 m	—	179 m)	—
$FeCl_2(DMU)_3$	280 vs	(255 vs	—	203 m)		353 s
$FeBr_3(DMU)_3$	220 s			220 s		354 s
$FeCl_2(BUA)_3$	285 s			220 w		368 s
$FeCl_2(MU)_6$	—			234 m 196 m		360 s
$FeCl_2(FA)_4$	(200-275 cm^{-1} broad unresolved absorption)					

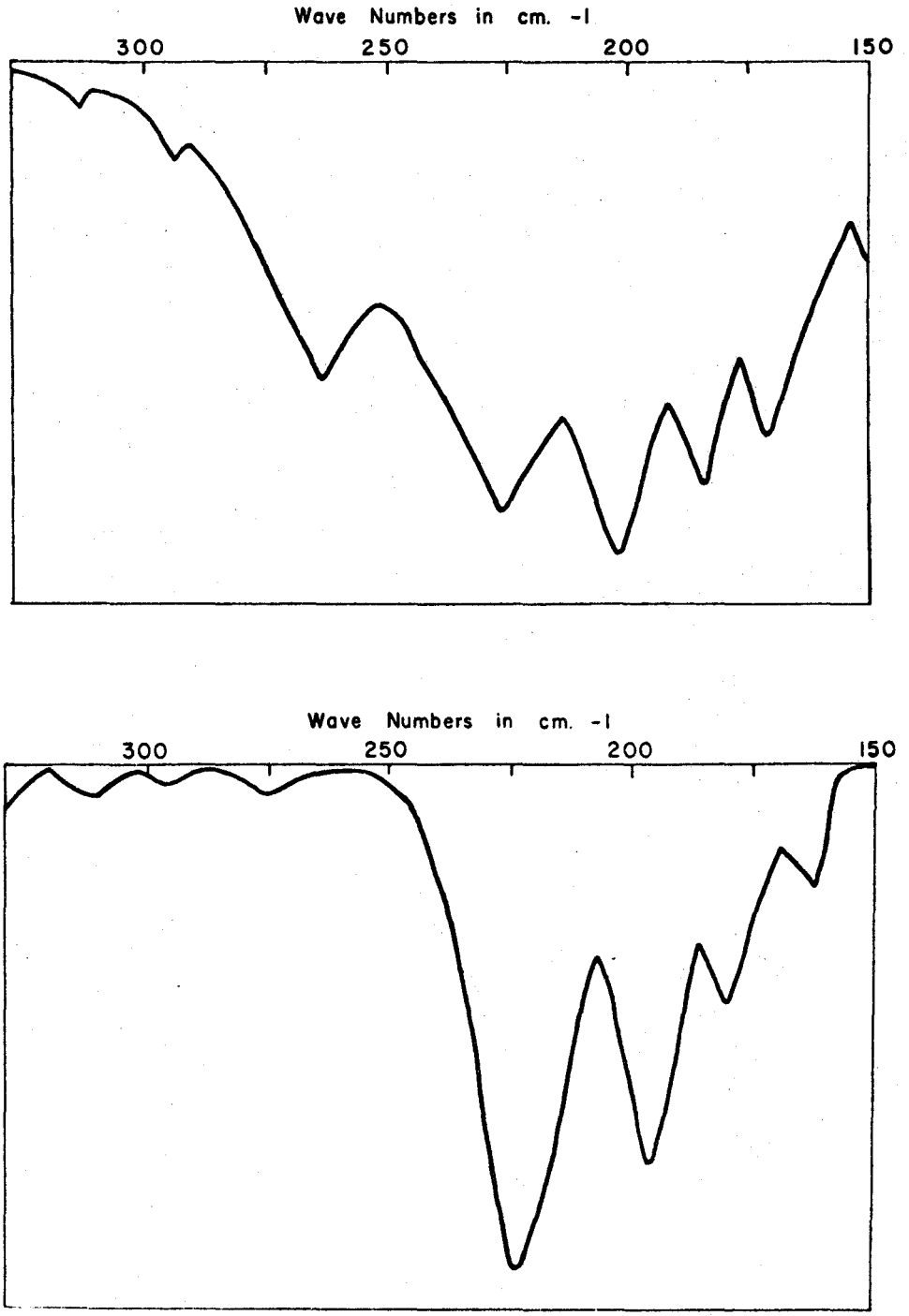

Figure 19. Far infrared spectra of $FeCl_2(AM)_2$ (top), and $FeCl_2(DMFA)_2$ (bottom).

It is noteworthy at this point to mention the ν(Fe-Cl) and ν(Fe-O) band assignments made by Singh and Rivest (18) for $FeCl_2(FA)_2$, $FeCl_2(MFA)_2$ and $FeCl_2(AM)_2$. These workers find Fe-Cl stretches between 350 and 380 cm^{-1}. On the grounds of assignments made in the present study and also other studies from the literature (43-45), it is thought that this region is too high for Fe-Cl stretching in iron II complexes, even if these complexes were tetrahedral as was claimed by Singh and Rivest (18). Rather, Fe-Cl stretching in this region is indicative of iron III, and it is suggested that the complexes may have been at least partially oxidized. Assignment of Fe-O stretching between 400 and 475 cm^{-1} by these workers is also questioned. Little information is available on iron II complexes with oxygen coordinating ligands. However, Kermarrec (76) reports Fe-O stretching at 357 cm^{-1} for $[Fe(H_2O)_6][SiF_6]$. Coordinate bonds with amides would be expected to be weaker than with water as a result of lower Lewis basicity, and ν(Fe-O) absorption should accordingly be at lower frequency.

The 1:1 benzamide complex shows a peak pattern very similar to that observed for the 1:2 complexes except for the appearance of a peak at 291 cm^{-1}. The peaks between 180 cm^{-1} and 260 cm^{-1} are interpreted as ν(Fe-O) and bridged ν(Fe-Cl) vibrations, as for the 1:2 complexes, and this is in keeping with the polymeric structure proposed for this complex (Fig. 16B). The peak at 291 cm^{-1}, however, suggests that at least one of the Fe-Cl bonds is short and has essentially non-bridged character.

The complex $FeCl_2(DMU)_3$ shows a peak at 280 cm^{-1} which is attributable to free Fe-Cl stretching as well as peaks at 255 cm^{-1} and 203 cm^{-1} attributable to bridged Fe-Cl stretching and Fe-O stretching. This is in

agreement with the proposed structure of this complex (Fig. 16A). The analogous bromide complex shows a single band at 220 cm^{-1} which is probably a strongly coupled Fe-Br and Fe-O stretching mode. Absorption due to bridged bromine bonds is expected to occur below 200 cm^{-1} (44).

The 1:4 formamide complex shows only broad, unresolved absorption between 200 and 275 cm^{-1} in the far infrared. Although Fe-Cl stretching is expected to occur in this region for monomeric octahedral complexes (p. 33), no further interpretation was possible. $FeCl_2(MU)_6$ shows two peaks at 234 and 196 cm^{-1}. If this complex is $[Fe(MU)_6]Cl_2$ as proposed then these must be Fe-O vibrations. The isobutyramide complex, formulated as $[Fe(BUA)_6][FeCl_4]$, shows a strong peak at 285 cm^{-1} assigned as ν(Fe-Cl) and a weak peak at 220 cm^{-1} assigned as ν(Fe-O). Clark and Dunn (45) observe ν(Fe-Cl) at 282 cm^{-1} in $[NEt_4]_2[FeCl_4]$.

Tables XIV - XXII show the infrared spectra in the region 1000-4000 cm^{-1} of the amide and urea ligands and complexes. Since the region from 400 to 1000 cm^{-1} provided little in the way of useful structural information the bands in this region have not been included. Whenever possible, the ligand spectra were recorded in dioxane solution, as well as in neat or mulled form, to show the effect of hydrogen bonding on the infrared absorption. Significant shifts to lower frequency are seen, particularly in the N-H and C=O stretching bands, on going from a dilute solution of the ligand to the neat or mulled form. Interpretation of peak shifts in the complexes due to coordination of the ligands will therefore be most valid if comparisons are made between the complex and its ligand in dilute solution. Band assignments from the literature are given for formamide, N-methylformamide, N,N-dimethylformamide, acetamide and urea. Tentative assignments are made in the other ligand spectra.

Four regions of the infrared are of significance in interpreting these spectra: the N-H stretching region, the C=O stretching region, the NH_2 bending region and the C-N stretching region. In all the amide and urea complexes peaks in the N-H stretching region are not significantly shifted to lower frequency, as would occur if coordination of the ligand were through nitrogen. The urea and substituted urea complexes show no change in the overall peak pattern in this region, as would be expected if coordination were through one of the nitrogens. This is particularly evident in the N,N'-dimethylurea case. Only one strong N-H stretching band is seen both in the ligand and its complexes. A further general observation in the N-H stretching region is that bands in the complex are often somewhat lower than the corresponding bands in a dilute solution of the ligand, but higher than in the neat or mulled ligand. This suggests that some hydrogen bonding is still effective in the coordinated ligand. Singh and Rivest (18) suggest that hydrogen bonding may occur between the amido hydrogens and the halide.

Carbonyl bands are in all cases shifted to lower frequency, giving firm evidence of oxygen coordination in these complexes. These shifts are 30 - 60 cm^{-1} in magnitude. Negative shifts in NH_2 bending frequencies are observable in all except the N-methylformamide complex, and this gives indirect support to coordination through oxygen (p. 35).

Bands of C-N stretching character are expected to shift to higher frequency if coordination takes place through oxygen. This is observable in all except the N,N-dimethylformamide complex where the peak at 1500 cm^{-1}, assigned as ν(C-N) in the ligand, appears at 1490 cm^{-1} in the complex. Infrared evidence, then, is fairly conclusive of coordination through oxygen in all the amide and urea complexes.

Table XIV. Infrared Spectra, 1000-4000 cm^{-1}, of Formamide and its Complexes.

Assignment*	Fa 0.2 M in dioxane	Fa neat	$FeCl_2(FA)_2$ mull	$FeCl_2(FA)_4$ mull
ν(N-H)	3574 w	—	—	—
	3435 m	3400 s	3392 m	3385 m
	3335 m	broad	3263 m	3290 m
	3285 sh	unresolved	3224 sh	3225 sh
	3235 sh	3275 s	3150 w	—
ν(C-H)	—	2886 m	2917 w	—
ν(C=O)	1707 vs	1684 vs	1688 s	1698 m
	—	—	1656 s	1684 m
	—	—	—	1652 s
δ(NH)	1607 w	1601 m	1586 m	1584 m
$\delta(CH)_{\text{in plane}}$	1391 m	1389 m	1373 m	1373 m
ν(C-N)	1310 m	1307 m	1347 w	1335 w
	—	—	1335 sh	1322 sh
$\delta(CH)_{\text{out of plane}}$	—	1080 sh	—	1075 w
	—	1048 w	—	1065 w

*Reference 53.

Table XV. Infrared Spectra, 1000-4000 cm^{-1}, of N-methylformamide and $FeCl_2(MFA)_2$.

Assignment*	MFA 0.2 M in dioxane	MFA neat	$FeCl_2(MFA)_2$ mull
ν(N-H)	3575 m	—	—
	3508 m	3480 sh	—
	3362 s	3295 s	3348 s
	—	3065 m	—
ν(C-H)	—	2940 m	—
	—	2878 m	—
ν(C=O)	1691 vs	1672 vs	1660 s
	—	—	1644 s
$\delta(NH_2)$	1531 m	1545 m	1544 m
$\delta(N\text{-}CH_3)$	1410 w	1414 m	1398 m
$\delta(CH)_{\text{in plane}}$	1388 m	1385 s	1370 s
ν(C-N)	1220 w	1244 m	—
$\rho(N\text{-}CH_3)$	—	1149 m	—
$\delta(CH)_{\text{out of plane}}$	—	1015 w	—

*Reference 77.

Table XVI. Infrared Spectra, 1000-4000 cm^{-1}, of N,N-dimethylformamide and $FeCl_2(DMFA)_2$.

Assignment*	DMFA 2 M in dioxane	DMFA neat	$FeCl_2(DMFA)_2$ mull
ν(C=O)	1677 vs	1670 vs	1642 s
	—	—	1614 s
ν(C-N)	1500 m	1503 s	1490 m
δ_a(N-CH_3)	—	1441 s	1446 s
δ_s(N-CH_3)	1410 m	1408 sh	—
δ(CH) in plane	1389 s	1390 s	1375 s
ν_a(C-N-C)	—	1258 s	1249 s
ω(N-CH_3)	—	1152 w	1155 w
ρ(N-CH_3)	—	1095 s	1117 s
	—	1067 m	1047 m

*Reference 52.

Table XVII. Infrared Spectra, 1000-4000 cm^{-1}, of Acetamide and its Complexes.

Assignment*	AM 0.2 M in dioxane	AM mull	$FeCl_2(AM)_2$ mull	$CuCl_2(AM)_2$* mull
ν(N-H)	3448 m	—	3385 s	—
	3346 m	3345 s	3310 sh	3373
	3221 w	3155 s	3262 m	3260
ν(C=O)	1706 s	1686 s	1677 s	1664
	1683 s	—	1657 s	—
δ(NH_2)	1617 m	1636 m	1582 m	1590
δ_a(CH_3)	—	1458 w	—	—
ν(C-N)	1380 m	1382 s	1408 m	1412
δ_s(CH_3)	—	1320 sh	—	1364
ρ(NH_2)	—	1148 s	1128 w	1134
γ(CH_3)	—	1043 w	1040 vw	1045
ρ(CH_3)	—	1002 w	—	1019

*Reference 78.

Table XVIII. Infrared Spectra, 1000-4000 cm^{-1}, of Urea and its Complexes.

Assignment*	UREA mull	$FeCl_2(UREA)_2$ mull	$[Fe(UREA)_6]Cl_3$ mull
ν(N-H)	3432 s	3467 s	3440 s
	3334 s	3395 s	3340 s
	3200 s	3355 s	3190 m
ν(C=O)	1690 s	1660 m	1655 sh
+	broad	1635 s	1625 s
$\delta(NH_2)$	unresolved	1615 m	1570 s
	1580 s	1577 s	1555 s
ν(C-N)	1460 m	1480 s	1495 s
	1445 m	—	—
$\rho(NH_2)$	1148 s	1148 w	1170 m

*Reference 50.

Table XIX. Infrared Spectra, 1000-4000 cm^{-1}, of N-methylurea and $FeCl_2(MU)_6$.

Assignment*	MU 0.2 M in dioxane	MU mull	$FeCl_2(MU)_6$ mull
ν(N-H)	3570 sh	—	—
	3448 sh	3421 s	3433 s
	3370 s	3323 s	3310 s
	—	3206 sh	3130 sh
ν(C=O)	1690 s	1685 sh	1643 s
$\delta(NH_2)$	1613 m	1652 s	1603 s
δ(NH) + ν(C-N)	1545 m	1581 s	1579 s
$\delta(N-CH_3)$	—	1421 m	1417 m
ν(C-N) + δ(NH)	—	1355 m	1370 s
$\rho(N-CH_3)$	—	1168 m	1173 m
	—	1105 w	—

*Tentative assignments made with reference to infrared spectral assignments in N-methylthiourea (64) and N-methylacetamide (79).

Table XX. Infrared Spectra, 1000-4000 cm^{-1}, of N,N'-dimethylurea and its Complexes.

Assignment*	DMU 0.2 M in dioxane	DMU mull	$FeCl_2(DMU)_3$ mull	$FeBr_2(DMU)_3$ mull
ν(N-H)	3390 s	3329 s	3355 s	3360 s
	—	3163 m	—	—
ν(C=O)	1687 s	1620 s	1622 s	1621 s
	1655 sh	—	—	—
δ(NH)	1550 s	1570 sh	1584 m	1582 m
	—	1538 m	1515 m	1512 m
$\delta(N-CH_3)$	1414 m	1417 m	1408 m	1412 m
ν(C-N)	—	1268 m	1310 m	1312 m
$\rho(N-CH_3)$	—	1169 m	1196 m	1197 m
	—	—	1171 m	1170 m
$\nu(N-CH_3)$	—	1038 w	1037 w	1033 w

*Tentative assignments made with reference to infrared spectral assignments for urea (50) and N-substituted amides (77).

Table XXI. Infrared Spectra, 1000-4000 cm^{-1}, of Benzamide and $FeCl_2(BM)$.

Assignment	BM 0.2 M in dioxane	BM mull	$FeCl_2(BM)$ mull
ν(N-H)	3442 s	—	3454 m
	3362 sh	3361 s	3342 m
	3328 s	—	—
	3273 m	—	—
	3210 m	3161 s	—
ν(C=O)	1683 vs	1660 s	1657 vs
Phenyl	1615 m	1622 s	1604 m
$\delta(NH_2)$	1580 m	1579 s	1564 s
	—	1451 m	1453 s
ν(C-N)	—	1398 s	1432 m
	—	1298 m	1300 m
$\rho(NH_2)$	—	1178 w	—
	—	1144 m	—
	—	1122 m	—

Table XXII. Infrared Spectra, 1000-4000 cm^{-1}, of Isobutyramide and $[Fe(BUA)_6][FeCl_4]$.

Assignment	BUA 0.2 M in dioxane	BUA mull	$[Fe(BUA)_6][FeCl_4]$ mull
ν(N-H)	3576 m	—	—
	3448 s	—	3384 sh
	3342 s	3350 s	3312 s
	3218 sh	3175 s	3260 m
	—	—	3190 m
ν(C=O)	1690 s	1665 sh	1651 s
$\delta(NH_2)$	1616 m	1636 s	1590 m
	—	—	1565 sh
	1470 m	—	1470 m
	1395 m	1435 m	1440 m
	1375 m	1365 m	1369 m
ν(C-N)	—	1295 s	1315 m
$\rho(NH_2)$	—	1168 w	1168 w
	—	1145 m	1130 m
	—	1088 m	1086 m

Table XXIII. Magnetic Moments of Amide and Urea Complexes.

Complex	Temperature	μ_{eff} (β)
$FeCl_2(AM)_2$	295°K	5.50
	77°K	5.32
$FeCl_2(UREA)_2$	295°K	5.45
	77°K	5.01
$FeCl_2(MFA)_2$	295°K	5.63
$FeCl_2(FA)_4$	295°K	5.46
	77°K	4.84
$FeCl_2(BM)$	295°K	5.34
	77°K	4.95
$FeCl_2(DMU)_3$	295°K	5.42
	77°K	5.04
$FeCl_2(MU)_6$	295°K	5.45
	77°K	4.93

Magnetic Moments

The magnetic moments of some of the amide and urea complexes are shown in Table XXIII. The room temperature moments are for the most part much larger than the spin only magnetic moment of 4.90 β. This indicates considerable spin-orbit coupling, as is expected to occur in high spin octahedral iron II compounds in which the splitting in the t_{2g} levels is not large.

In all the complexes except $FeCl_2(AM)_2$ the magnetic moments show an abnormally large temperature dependence, dropping to values at 77°K which are near the spin only values. Golding et al (80) have calculated the temperature dependence of the magnetic moment of high spin iron II for various values of Δ, the distortional splitting in the t_{2g} levels, and λ, the spin-orbit coupling constant. Their calculation is based on the assumption that Δ and λ themselves do not vary with temperature. From their calculated curves it would appear that for moderate Δ values considerable orbital contribution to the magnetic moment should remain at 77°K. It is therefore suggested that there may be some temperature dependence of Δ and/or λ in the present cases.

Golding et al (80) have also calculated the relationship between magnetic moment and quadrupole splitting for high spin iron II compounds in which d_{xy} lies lowest. Their calculated curve for the room temperature case in which is given its free ion value is shown in Fig. 20. Some of the data from this study are placed on the plot. Agreement with the curve, even when errors of 0.05 mm/sec in the quadrupole splittings and 0.05 in the magnetic moments are allowed, is not especially good, likely indicating that the assumption of free ion spin-orbit coupling is a poor one.

Figure 20. Relationship between quadrupole splitting and magnetic moment for high spin ferrous compounds with d_{xy} ground state.

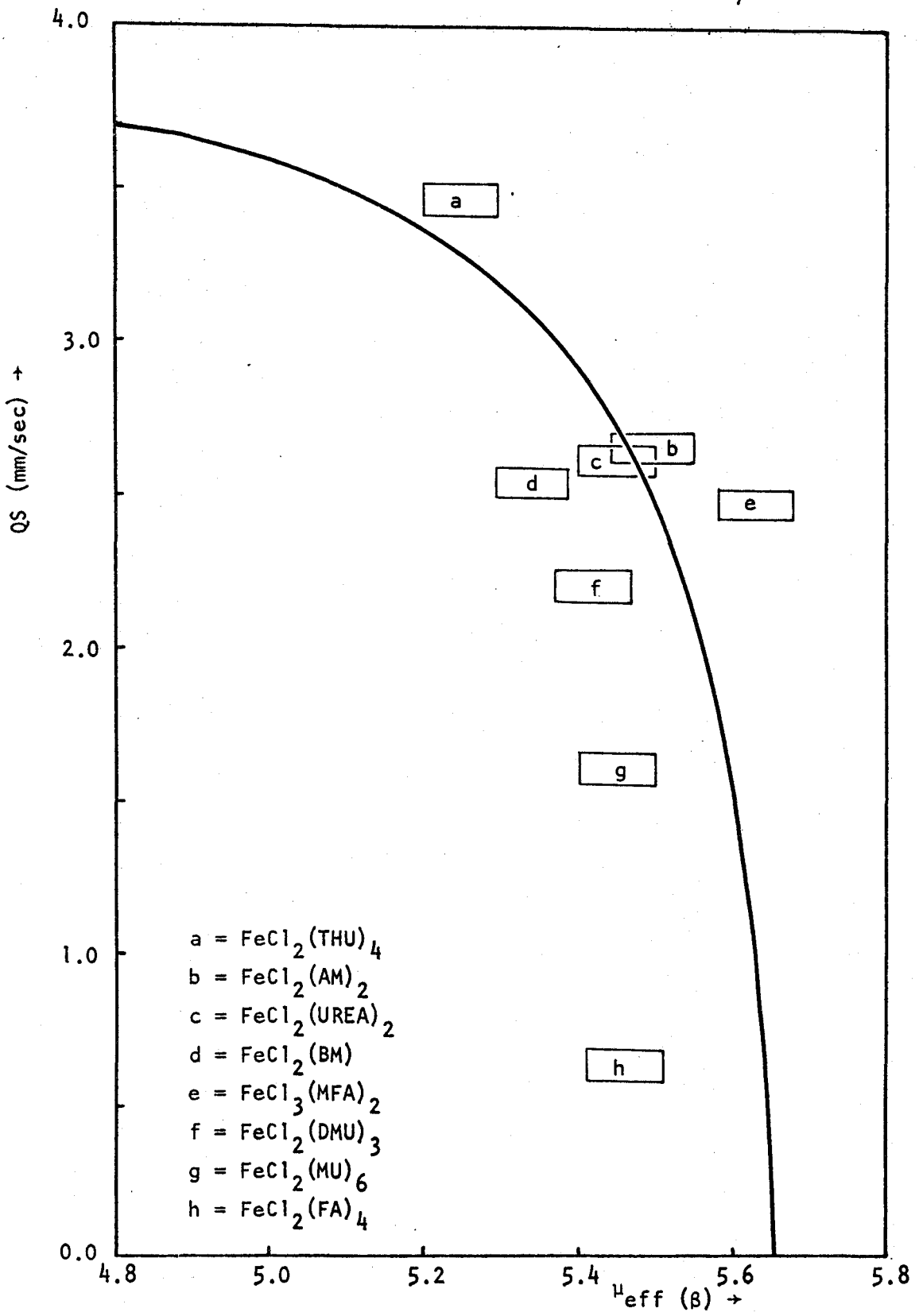

The 1:4 formamide and 1:6 N-methylurea complexes lie well inside the curve, and as suggested earlier (p. 87, 89) these complexes may have a d_{xz}, d_{yz} rather than a d_{xy} ground state. The N-methylformamide complex lies well outside the curve, perhaps due to partial oxidation of the sample.

Complete temperature runs would have been valuable in a comparison such as this, and would have led to specific values for Δ and λ as well as confirming any temperature dependence of these parameters.

CONCLUSION

A number of complexes FeX_2L_2 have been prepared, and it has been possible to divide these into two structural types on the basis of their Mossbauer, far infrared spectra, and magnetic properties. The complexes in which L is a sulfur-coordinating ligand (thioacetamide, thiourea, N-methylthiourea and N,N'-dimethylthiourea) are thought to form monomeric tetrahedral complexes. This group shows Mossbauer isomer shifts close to 1.00 mm/sec, in the region expected for 4-coordinate iron II. The far infrared spectra show strong, well-resolved Fe-Cl stretching bands close to 300 cm^{-1} and FeBr stretching bands close to 250 cm^{-1}, these regions again indicative of 4-coordinate structures. The magnetic moments are close to the spin only value of 4.90 β for high spin iron II. The Mossbauer quadrupole splittings are in all cases greater than 3.0 mm/sec, indicating ligand fields which are considerably distorted from cubic symmetry. The distortional splitting in the e levels has been estimated to be about 800 cm^{-1}. The complexes FeX_2L_2 in which X = Cl and L is a ligand coordinating through oxygen (formamide, N-methylformamide, N,N-dimethylformamide, acetamide and urea) are thought to be chlorine bridged polymers with octahedral coordination about iron. Isomer shifts are close to 1.4 mm/sec, in the region expected for 6-coordinate iron II. The far infrared spectra show no bands close to 300 cm^{-1}, but a number of poorly resolved bands between 260 and 180 cm^{-1}. The magnetic moments are close to 5.45 β, suggesting a t_{2g} ground state with a fairly large degree of spin-orbit cou ling. An abnormally large temperature dependence of the magnetic moment has been observed in all

except the acetamide complex, and it is suggested that either the spin-orbit coupling constant or the distortional splitting in the t_{2g} levels, or both, may vary with temperature. The quadrupole splittings are between 2.5 and 3.0 mm/sec at room temperature and increase only slightly at 77°K.

Two complexes $FeCl_2L_4$ (L = thiourea, formamide) have been investigated. Infrared spectra show these to be sulfur-coordinated and oxygen-coordinated respectively. Both have been assigned monomeric octahedral structures. The formamide complex has the larger isomer shift, indicating less covalent character in the bonds, as expected. Its quadrupole splitting is very small for a high spin iron II complex, only 0.66 mm/sec at room temperature. It is suggested that (i) this complex has a near cubic environment about iron and (ii) that it has a d_{xz} or d_{yz} ground state. The thiourea complex, in contrast, has the largest quadrupole splitting observed in this study, 3.46 mm/sec at room temperature, indicating a highly distorted octahedral environment and a d_{xy} ground state. Its magnetic moment of 5.25 β supports the above proposal.

Two complexes $FeCl_2L$ (L = benzamide, aniline) are thought to form extensively cross-bridged polymers with 5 chlorines and one ligand about each central iron. The isomer shifts of these complexes are about 1.4 mm/sec and this is thought to rule out the possibility of dimeric chlorine bridged structures with tetrahedral coordination.

1:3 complexes $FeCl_2L_3$ (L = N,N'-dimethylurea) and $FeBr_2L_3$ (L = N,N'-dimethylurea, aniline) have been assigned halogen bridged dimeric structures. Isomer shifts show these to be 6-coordinate. The bromides

have smaller isomer shifts, showing them to have greater covalency in their bonds. A far infrared spectrum of the chloride complex shows absorption both in the 300 cm^{-1} region characteristic of Fe-Cl bonds and in the 260-180 cm^{-1} region characteristic of bridged Fe-Cl bonds, and this further supports the structural assignment.

Another 1:3 complex $FeCl_2$(isobutyramide)$_3$ was shown by its Mossbauer spectrum to have two iron centres, one 4-coordinate and one 6-coordinate. An ionic structure $[Fe(BUA)_6][FeCl_4]$ is proposed. The far infrared spectrum shows two peaks, at 285 and 220 cm^{-1}, assigned as Fe-Cl and Fe-O stretching respectively. Quadrupole splittings for both species were fairly small, showing them to have near cubic symmetry. For the tetrachloroferrate anion a distortional splitting in the e levels of 185 cm^{-1} was estimated.

A 1:6 complex $FeCl_2$(N-methylurea)$_6$ gave isomer shift and quadrupole splitting values close to those observed for the $Fe(BUA)_6^{2+}$ cation. This complex has been formulated as $[Fe(MU)_6]Cl_2$. It shows one peak in the far infrared at 234 cm^{-1}, assigned as Fe-O stretching.

REFERENCES

1. D. Goodgame, M. Goodgame, M. Hitchman and M. Weeks, Inorg. Chem. 5, 635 (1966).
2. D. Forster and D. M. L. Goodgame, J. Chem. Soc., 454 (1965).
3. N. N. Y. Chan, M. Goodgame and M. J. Weeks, J Chem. Soc. (A), 2499 (1968).
4. F. A. Cotton and M. D. Meyers, J. Am. Chem. Soc. 82, 5023 (1960).
5. T. C. Gibb and N. N. Greenwood, J. Chem. Soc., 6989 (1965).
6. C. Furlani, E. Cervone and V. Valenti, J. Inorg. Nucl. Chem. 25, 159 (1963).
7. N. S. Gill, J. Chem. Soc., 3512 (1961).
8. D. Forster and D. M. L. Goodgame, J. Chem. Soc., 268 (1965).
9. P. R. Edwards, C. E. Johnson and R. J. P. Williams, J. Chem. Phys. 47, 2074 (1967).
10. D. Forster and D. M. L. Goodgame, J. Chem. Soc., 454 (1965).
11. J. C. Sheldon and S. Y. Tyree, J. Am. Chem. Soc. 80, 4775 (1958).
12. M. J. Frazer, W. Gerrard and R. Twaits, J. Inorg. Nucl. Chem. 25, 637 (1963).
13. C. D. Burbridge and D. M. L. Goodgame, J. Chem. Soc. (A), 1074 (1968).
14. C. D. Flint and M. Goodgame, J. Chem. Soc. (A), 750 (1968).
15. M. Nardelli and I. Chierici, Gazzetta 87, 1478 (1957).
16. M. Nardelli, G. F. Gasparri, A. Musotti and A. Manfredotti, Acta Cryst. 21, 910 (1966).
17. M. Nardelli, L. Cavalca and A. Braibanti, Gazzetta 86, 867 (1957).

18. P. P. Singh and R. Rivest, Can. J. Chem. 46, 1773 (1968).

19. T. Birchall, Can. J. Chem. 47, 1351 (1969).

20. R. L. Mossbauer, A. Physik 151, 124 (1958).

21. R. L. Mossbauer, Naturwiss. 45, 538 (1958); Z. Naturforsch. 14a, 211 (1959).

22. C. Kittel, "Introduction to Solid State Physics," Wiley, New York, 1956, Ch. 5, 6.

23. A. J. F. Boyle and H. E. Hall, Rept. Progr. Phys. 25, 441 (1962).

24. G.K. Wertheim, "Mossbauer Effect: Principles and Applications," Academic Press, New York, 1964.

25. B. D. Josephson, Phys. Rev. Letters 4, 342 (1960).

26. R. V. Pound and G. A. Rebka, Jr., Phys Rev. Letters 4, 274 (1960).

27. T. C. Gibb, R. Greatrex and N. N. Greenwood, J. Chem. Soc. (A), 891 (1968).

28. V. I. Goldanskii, E. F. Makarov and V. V. Khrapov, Phys. Letters 3, 344 (1963).

29. V. I. Goldanskii, E. F. Makarov and V. V. Knrapov, Soviet Phys. J. E. T. P. 17, 508 (1963).

30. S. V. Karyagin, Doklady Akad. Nauk S. S. S. R. 148, 1102 (1963).

31. M. Blume, Phys Rev. Letters 14, 96 (1965).

32. A. P. Ginsburg and M. B. Robin, Inorg. Chem. 2, 817 (1963).

33. L. R. Walker, G. K. Wertheim and V. Jaccarino, Phys Rev. Letters 6, 98 (1961).

34. C. D. Burbridge and D. M. L. Goodgame, J. Chem. Soc. (A), 694 (1967).

35. C. D. Burbridge, D. M. L. Goodgame and M. Goodgame, J. Chem. Soc. (A), 349 (1967).

36. J. F. Duncan, R. M. Golding and K. F. Mok, J. Inorg. Nucl. Chem. 28, 1114 (1966).

37. E. Fluck, "The Mossbauer Effect and Its Applications in Chemistry," Adv. Inorg. Chem. & Radiochem. 6.

38. V. I. Goldanskii, "The Mossbauer Effect and Its Applications in Chemistry," Consultants Bureau, N. Y. 1964.

39. R. Ingalls, Phys. Rev. 133A, 787 (1964).

40. C. J. Ballhausen, "Introduction to Ligand Field Theory," McGraw-Hill, New York, 1962.

41. T. C. Gibb, J. Chem. Soc. (A), 1439 (1968).

42. K. Ono and A. Ito, J. Phys. Soc. Japan 19, 899 (1964).

43. R. J. H. Clark, Spectrochem. Acta 21, 955 (1965).

44. R. J. H. Clark and C. S. Williams, Inorg. Chem. 4, 350 (1965).

45. R. J. H. Clark and T. M. Dunn, J. Chem. Soc., 1198 (1963).

46. A. Sabatini and L. Sacconi, J. Am. Chem. Soc. 86, 17 (1964).

47. C. D. Flint and M. Goodgame, J. Chem. Soc. (A), 744 (1966).

48. J. F. Duncan and K. F. Mok, Australian J. Chem. 19, 701 (1966).

49. C. M. Lee and W. D. Kumler, J. Am. Chem. Soc. 84, 571 (1962).

50. R. B. Penland, S. Mizushima, C. Curran and J. V. Quagliano, J. Am. Chem. Soc. 79, 1575 (1957).

51. J. E. Stewart, J. Chem. Phys. 26, 248 (1957).

52. R. L. Jones, J. Mol. Spectry. 11, 411 (1963); ibid. 2, 581 (1958).

53. J. C. Evans, J. Chem. Phys. 22, 1228 (1954).

54. K. Nakamoto, "Infrared Spectra of Inorganic and Coordination Compounds," John Wiley & Sons, New York, 1963.

55. J. Chatt, L. A. Duncanson and L. M. Venanzi, J. Chem. Soc., 2712 (1956).

56. P. Vaughan and J. Donohue, Acta Cryst. 5, 530 (1952).

57. R. Rivest, Can. J. Chem. 40, 2234 (1962).

58. R. C. Aggarwal and P. P. Singh, Z. anorg. allg. Chem. 332, 103 (1964).

59. R. C. Aggarwal and P. P. Singh, J. Inorg. Nucl. Chem. 26, 2185 (1964).

60. R. C. Aggarwal and P. P. Singh, J. Inorg. Nucl. Chem. 28, 1655 (1966).

61. I. Suzuki, J. Chem. Soc. Japan 35, 1449 (1962).

62. A. Yamagouchi, R. Penland, S. Mizushima, J. Lane, C. Curran and J. Quagliano, J. Am. Chem. Soc. 80, 527 (1958).

63. K. Swaminathan and H. M. N. H. Irving, J. Inorg. Nucl. Chem. 26, 1291 (1964).

64. T. J. Lane, A. Yamagouchi, J. V. Quagliano, J. A. Ryan and S. Mizushima, Am. Chem. Soc. 81, 3824 (1959).

65. R. S. Drago, D. W. Meek, M. D. Joesten and L. LaRoche, Inorg. Chem. 2, 124 (1963).

66. A. I. Vogel, "Quantitative Inorganic Analysis," Longmans, Green & Co., New York, 1951.

67. A. Guest, Ph.D. thesis, Department of Chemistry, McMaster University, Hamilton, Ontario, September, 1968.

68. N. S. Gill, R. S. Nyholm, G. A. Barclay, T. I. Christie and P. J. Pauling, J. Inorg. Nucl. Chem. 18, 88 (1961).

69. K. Ono and A. Ito, J. Phys Soc. Japan 19, 899 (1964).

70. A. J. Nozik and M. Kaplan, Phys. Rev. 159, 273 (1967).

71. D. M. L. Goodgame, M. Goodgame, M. A. Hitchman and M. J. Weeks, Inorg. Chem. 5, 635 (1966).

72. C. E. Johnson, Proc. Phys. Soc. (London) 88, 943 (1966).

73. B. Morosin and E. J. Graeber, J. Chem. Phys. 42, 898 (1965).

74. R. W. Grant, H. Wiedersich, A. H. Muir, Jr., U. Gonser and W. N. Delgass, J. Chem. Phys. 45, 1015 (1966).

75. B. R. Penfold and J. A. Grigor, Acta Cryst. 12, 850 (1959).

76. Y. Kermarrec, Comp. rend. 258, 5836 (1964).

77. T. Miyazawa, T. Shimanouchi and S. Mizushima, J. Chem. Phys. 24, 408 (1956).

78. W. Kutzelnigg and R. Mecke, Spectrochim. Acta 18, 549 (1962).

79. T. Miyazawa, T. Shimanouchi and S. Mizushima, J. Chem. Phys. 29, 611 (1958).

80. R. M. Golding, K. F. Mok and J. F. Duncan, Inorg. Chem. 5, 774 (1966).